UCRL-17438

C.2

University of California

Ernest O. Lawrence Radiation Laboratory

COMBUSTION OF HEPTANE DROPLETS IN A HOT GAS FLOW

Joel Lawrence Bert
(M. S. Thesis)

October 1967

DISCLAIMER

UCRL-17438

UNIVERSITY OF CALIFORNIA

Lawrence Radiation Laboratory
Berkeley, California

AEC Contract No. W-7405-eng.48

COMBUSTION OF HEPTANE DROPLETS IN A HOT GAS FLOW

Joel Lawrence Bert

(M.S. Thesis)

October 1967

TABLE OF CONTENTS

COMBUSTION OF HEPTANE DROPLETS IN A HOT GAS FLOW

Joel Lawrence Bert

Inorganic Materials Research Division, Lawrence Radiation Laboratory,
Department of Chemical Engineering, University of California
Berkeley, California

October 1967

ABSTRACT

Burning rates of individual n-heptane droplets were measured under forced convective conditions and environmental temperatures of 550 to 700°C. The droplets were supported in a hot air stream rising at approximately their terminal velocity and their burning histories were recorded by high speed motion picture photography. From analysis of the photographs data on droplet size, convective velocities and burning rates were obtained. The effects of gas temperature, drop size, and convection on droplet burning rate coefficients were studied. In the size range studied, 100-500μ droplet diameter appeared to have no effect on burning rate coefficients. The coefficients were also not noticeably influenced by convection for relative velocities up to 90 cm/s. These results are in accord with predictions of simplified combustion models. However, the observed rate of increase of burning rate coefficient with increasing temperature between 550°C and 700°C was much greater than present combustion theory would predict, but is consistent with the few results of other investigators available for elevated environmental temperatures. These results indicate that additional phenomena influencing burning rates at elevated temperatures and/or convective conditions may have to be considered.

I. INTRODUCTION

Liquid fuels are commonly burned as sprays of liquid droplets in oxidizing atmospheres. The study of the evaporation and combustion of fuel droplets is thus a subject of considerable importance for describing combustion performance in many such devices as liquid fueled turbine engines and fired process heaters. The objective of this research is the experimental study of rapid evaporation and combustion of liquid fuel droplets under forced convective conditions in a heated gas stream. Droplet evaporation under these conditions is characterized by large radial velocities of the evaporating material at the drop surface.

In this work, the quasi-steady state combustion and evaporation rates are investigated by high speed motion picture photography of hydrocarbon droplets of 100-300μ diameter during evaporation and combustion in an air stream at temperatures up to 700°C.

A. Previous Work

The phenomena of droplet combustion and evaporation is characterized by simultaneous heat and mass transfer involving chemical reaction. The combination of these three phenomena and the interaction between them creates problems in the theoretical analysis. Theoretical analyses of the situation, for which early contributors include Godsave (1952),[1] Spalding (1953),[2] Goldsmith and Penner (1954),[3] Lorell and Wise (1955),[4] and Penner (1957),[5] have produced models which are quite similar. Common to their approaches are several assumptions. These are: spherical symmetry (stagnant environment), no radiant heat transfer from flame to drop, drop at uniform temperature corresponding to its boiling point, isobaric combustion, infinitely fast reaction kinetics (infinitesimally

thin reaction zone), and steady state evaporation and combustion. Williams[6] analyzed several of these assumptions and concluded that the radiant heat transfer is negligible but that the assumption of constant temperature of the drop is good only for high energy fuels. He also concluded that the boiling point temperature assumption of the drop is only fair for low energy fuels. Concerning the steady state assumption, Williams concluded that this may cause errors of up to 20% for evaporation and combustion rates.

The assumption of spherical symmetry can only be true when there is no convection; natural or forced. Lorell, Wise and Carr[7] present an analysis which investigates the assumption of infinite reaction rates.

A principal result of the theoretical analyses is that the mass burning rate of a droplet is proportional to the diameter of the droplet. An alternative way of expressing this is that the rate of decrease of the diameter squared of the droplet is proportional to time. The negative constant of proportionality of this decrease is called the burning rate coefficient. Also, from the theoretical investigation temperature profiles and flame radius can be predicted.

Among the first experimental measurements of droplet evaporation and combustion was the work carried out by Godsave.[1] He burned sixteen different fuels including n-heptane. The fuels were suspended as drops on a silica filament. Several other experimental investigators also chose to investigate droplets under this situation.[8,9,10] In Godsave's experiment the drops were about 1500μ in diameter. A 16mm camera operating at four frames per second recorded the drop size change with time after the drop had been ignited and allowed to burn in air at room temperature. Because of the bright backlighting no evidence of the flame

was found on the film. From the photographic record of the diameter of the drop and time, Godsave was able to conclude that the mass rate of burning was proportional to the diameter of the droplet, a confirmation of the theoretical analysis. Godsave found a proportionality constant between diameter squared and time, or a burning rate coefficient, of 0.0097 cm^2/sec for n-heptane. He also concluded that the problem of heat transfer from the flame to the drop should be considered to be taking place in a radially moving medium because of the large radial velocities of the evaporating material.

Goldsmith[8] utilized more elaborate equipment in his experiments than did Godsave. He could regulate the temperature of the environment up to 1000°C and the pressure up to 5 atmospheres. During his experiments the oxygen concentration in the environment was varied from 23% to 90%. The drops were again suspended from silica filaments and were 1.5 to 1.8 mm in diameter (1500 to 1800μ). A 35mm camera operating at about 24 frames per second recorded the droplet diameter decrease with time. The results here were again a confirmation of the linear burning law. For n-heptane the burning rate coefficient in air at room temperature and atmospheric pressure was 0.0084 cm^2/sec, which is in fair agreement with Godsave's experimental results and very good agreement with those of Goldsmith and Penner[3] (0.0086 cm^2/sec). The theoretical analysis as presented by Goldsmith and Penner is basically under the same conditions as explained earlier.

Goldsmith also reported on some effects of forced convection. For this experimental work he suspended droplets from a quartz filament, the filament and drop being in turn suspended in a channel where the air flow rate could be adjusted. For an air velocity of 34.5 cm/sec the

ratio of the burning constant for n-heptane under forced convection to that under still air was 1.36. He lastly presented a relationship between theoretical burning rate coefficients and temperature which shows an increase in burning rate coefficient of about 20% from 300°K to 1050°K.

Bolt and Saad[11] in their experimentation were concerned with the influence of convection on burning droplets. The size range of the droplets used was 300-1150μ. The drops were formed from a small bore tube, where the fuel was supplied, surrounded by a concentric jet of air. As the drops were formed at the tip of the tube, they were blown vertically down off of the tip of the tube by the air jet. The drops then fell through a furnace whose maximum attainable temperature was 1700°F. Four cameras were positioned vertically along the furnace with open shutters. As the drop fell into the field of view of each, a photo multiplier tube triggered a strobe photolight (1μ sec) to photograph the drop. One of the camera positions was not used because the temperature at this position was lower than in the rest of the furnace. Since only three data points could be obtained from any one run, different size droplets were used in several runs, and the results combined in a record of diameter squared versus time. From this, a burning rate coefficient for n-heptane of 0.0195 cm^2/sec was obtained. This value is much higher than any cited by other investigators. From this experiment it was difficult to determine the effect of forced convection on combustion because of the fact that there was an insufficient number of data points for each drop considered.

Kumagai and Isoda[9] tried to eliminate the effects of natural convection by observing combustion during free fall. A droplet was mounted on a silica filament in a wooden box. The chamber was supported on a cable over a pulley and counterbalanced so that its acceleration could be

varied from zero to the acceleration due to gravity. A schlieren photographic system was provided along the path of the falling chamber. The size of the drops that were studied were 1000μ to 1500μ. For n-heptane a burning rate coefficient of 0.0060 cm^2/sec was observed when the gravity effect was zero. This is considerably lower than burning rate coefficients reported by other investigators under natural convection. Kumagai and Isoda observed that under zero gravity the drops and the flame front were spherical as opposed to the natural convection case where the flame is elongated upwards. This convection free situation yielded experimental results for the burning rate coefficient that were 60% of the accepted theoretical results.

In an important work Ingebo,[12] working with sprays, suggested that the heat transferred to burning sprays as based on the areamedian drop diameter agreed with the heat transferred to non-burning drops evaporating in an air stream. This agreement came in the form of similar overall heat transfer coefficients. In the same article he offered correlations of the reduced drag coefficients on burning drops, a phenomena that has been noticed previously.

Agoston, Wise and Rosser[13] employed a porous sphere in their experiments dealing with the influence of convection on burning. The advantage of this procedure is that the mass burning rate of the wetted sphere can be determined by the amount of material that must be continuously supplied to the sphere in order to maintain a wet surface without any excess fuel being shed. Other experimenters have also chosen this technique.[2,14,15] Agoston, Wise and Rosser, working with spheres of 0.3 to 1.3 cm in diameter, concluded that the mass burning rate of the drops increased as the velocity of the gas stream increased

up until the extinction velocity (that velocity of gas which extinguishes the flame). For an increase in the mass burning rate of ethyl alcohol burning at room temperature by a factor of 1.36, an air velocity of about 40cm/sec would have to be applied. They developed relationships of the mass burning rate of a sphere versus the air velocity for n-butanol, ethyl alcohol and benzene and showed an increase in burning rate coefficient with convection of up to 100% over the natural convection case.

Important variables that have been studied in connection with droplet evaporation and combustion are: temperature, pressure, gas composition and relative velocity of gas (convection). Some of the more important features of droplet evaporation and combustion that have received attention are: burning rate coefficients, ignition time lag and distance of flame surface from the drop.

B. Perspective

The experimental technique employed in this work hopes to simulate, more closely than in previous work, the convective conditions under which droplets are burned in situations of practical interest.

The situation of the droplets in this experiment is such that there is no influence of filaments or porous spheres to interfere with the actual heat transfer or fluid mechanics of the burning. In actual situations, droplets are burned in the form of sprays. As these sprays burn, hot gas from the combustion process expands. This acceleration of the hot gas carries the droplets in a convective flow field where they travel at approximately their terminal velocity with respect to the gas. It is this situation that is being simulated in this experimental work rather than combustion and evaporation under situations of natural convection or no convection at all.

A metered gas stream, of controllable composition, is heated and passed in laminar flow up a rectangular flow channel. At the bottom of this vertical channel is the droplet injection mechanism. The drops, of approximately 100-300μ in diameter, are injected vertically upward into the heated gas stream with a velocity greater than that of the flowing gas. At the top of this column is a section with transparent diverging walls where the velocity of the gas decreases. By the time a drop of the appropriate size reaches this height it has lost its initial momentum and is at terminal velocity with respect to the moving gas. Consequently, certain size droplets are suspended in this diverging section, their size being determined by the velocity of the gas in this test section. The parabolic velocity profile across the test section serves to center any droplets that stray off of center. A drop in contact with the heated gas stream autoignites and, by the time it reaches the top of the column, is in a quasi-steady combustion. A high speed motion picture camera mounted at the test section is used to record droplet combustion.

II. EXPERIMENTAL DESIGN

This investigation is carried out with the purpose of examining the evaporation and combustion of hydrocarbon droplets in a convective environment. In order to accomplish this several requirements must be satisfied. These include: forming droplets, inserting these droplets in a hot convective environment, locating the droplets in a position where their evaporation and combustion can be recorded, and recording the course of combustion or evaporation of the droplets. The following sections describe the manner in which these requirements are fulfilled in this study. Most of the experimental design for this investigation was developed by Salabarria[16] in his previous work on the same project. The general concept of the experiment is to inject droplets into a stream of vertically flowing heated gas, which supports these droplets at a fixed height in a test section where a camera is focused to record the rates of evaporation and combustion of droplets.

A. Test Section

In order for burning of droplets to be recorded by a stationary camera, the droplets in turn must remain approximately stationary with respect to the camera. Since the purpose of this experimental work is to study the influence of convection on burning of drops, the drops must be moving with respect to the gas stream. A droplet falling in a gas stream under the influence of gravity will travel at its terminal velocity, which is determined by the size of the droplet and the conditions of the gas. If instead of the droplet falling, the gas is moving upward with the corresponding terminal velocity of the droplet, then the droplet will appear stationary. This condition necessitates a flow field with velocity changing with position in the direction of flow, so that a specific size droplet will reach a terminal velocity corresponding to the velocity of the gas at a given position. For droplets to remain stationary with respect to a fixed camera, their lateral

motion must also be suppressed. These requirements can be satisfied by a laminar flow field of the gas in a diverging wall test section. The parabolic velocity profile inherent in the laminar flow in a duct tends to stabilize droplets at the maximum velocity or at the center of the symmetric flow. The diverging walls provide a variable velocity flow field. By adjusting the angle of divergence of the walls in the test section, the rate at which the velocity decreases up the test section can be controlled. This adjustment along with control of the mass flow rate of the gas controls the size of the droplets to be suspended in the field of view of the camera. Salabarria[16] designed the test section for this investigation with a 40 cm duct that serves as an entrance length to the test section. This entrance length serves to insure well developed laminar flow by the time the gas reaches the test section, and also as a length over which injected drops lose their initial momentum. The separation of the diverging walls at the entrance of the test section was determined so that there will be a 1% change in velocity if a drop strays one diameter from the center of the parabolic velocity profile and so that the separation is at least one order of magnitude larger than the drops.

B. Droplet Injection

The experimental design behind this investigation demands that droplets be injected in a manner so that they reach the test section. Some considerations involved in forming the droplets are as follows: size of droplets, direction of entry of the drops into the test section, and number of drops to be formed. In order to provide accommodation of the droplets to the environment in which they are to be studied, Salabarria[16] decided to inject the drops vertically upward into the heated flowing gas stream. By injecting the droplets in this direction, they must traverse the entrance length which serves as a distance over which initial momentum can be lost. The greater the number of drops injected, the more the concentration of the gas stream will

be affected by combustion products and evaporated hydrocarbon. Conversely, the fewer droplets injected the less is the possibility of a burning droplet reaching the field of view of the camera. Therefore a compromise must be reached as to the number of drops formed. Not more than 100 drops of 300μ diameter are to be formed per run. The droplets are formed by forcing the fluid to be studied through a sharp edged orifice by the impulsive motion of a plunger. Varying the stroke distance of the plunger varies the number of drops that are formed. In order not to impart excessive momentum to the drops, the rate at which the plunger is moved is empirically determined so that drops reach the test section without excess momentum. The size of the drops that are formed is controlled by the size of the orifice, with the drop diameter being almost twice that of the orifice.

C. Heating the Gas Stream

The requirement of laminar gas flow in the test section, whose minimum cross sectional area is on the order of 2 cm^2, dictates a very low mass rate of gas flow. The gas must be continually heated over perhaps 900°C, a specification which when considered along with the limitations on heating element materials temperature (1200°C) constitutes a severe heat transfer problem. Large heat transfer areas cannot be readily heated by electrical resistance elements on a continuous basis. Reasonably high heat transfer coefficients require high gas velocities which, for a stationary heat transfer surface would generate excessive pressure drops in the gas stream. In developing the gas heating system used in this work, Salabarria[16] approached this problem by moving the heating surface at high velocities through the slowly moving gas. This is accomplished by mounting the heating elements in a rotating cylindrical array which is located in an enlarged section of the gas inlet channel. When this arrangement is rotated up to maximum rate of 800 RPM, high enough heat transfer coefficients (1-10 BTU/ hr. $ft.^2$°F)[16] can be realized so as to heat the required mass flow rates (2000-6000 cc/min at standard conditions) to the

necessary temperatures.

D. Photographic Equipment

The experimental design of this work has as its focal point the recording of droplet size as a function of time during evaporation and combustion. The history of free falling burning or evaporating drops can only be recorded by photographic means; in this case a high speed motion picture camera. If an average burning rate coefficient for n-heptane is about 0.01 cm^2/sec, then a 100μ drop will decrease in diameter to 10μ in 0.01 seconds. A lower limit of 10μ is chosen because below that size the linear burning law may not apply,[17] the lifetime of the drop from 10μ to complete vaporization is small when compared to 0.01 seconds, and photographing drops smaller than this presents severe problems. Hence the time available for photographing a 100μ drop is not more than 0.01 seconds. The maximum time available for photographing droplets larger than 100μ increases as the square of the drop diameter assuming that the droplets will stay in the field of view of the camera throughout their lifetime. It is assumed that a working estimate of minimum time available under perfect conditions for photographing an event is 0.01 seconds. The desired number of pictures of any event is around 30-100 this range being chosen so that the data would be statistically effective. These requirements dictate that the camera have the capability of working at frame rates on the order of a few thousand frames per second. The Fastax WF17 camera satisfies this requirement.

Because photographic means are employed in this investigation, special consideration of several of the optical consequences is warranted. Examples of these are: image magnification, depth of field of the camera, and illumination. Image magnification is very critical in this experiment because for accurate measurements of the drop diameter to be taken from the film the largest practicable magnifications are required. Magnifications greater

than 1:1 are required because of the resolving power of the film. The film of best resolving power usable in the Fastax without causing excessive peripheral problems was DuPont's 931A Rapid Reversal Panchromatic Film with a resolution of 100 lines per mm (10μ) as reported by the manufacturer. It is desired to have images on the film that are as large as possible so as to lessen the relative error inherent in the measurement. Magnifications employed in this work range from 1:1 to 2-1/2:1. However, the standard lenses available for the Fastax WF17 camera are not designed to be used at magnifications greater than 1:1. Lens abberations become noticeable in the image when magnifications of greater than 1:1 are used and the field of view of the camera must be calibrated to account for the distortion.

The depth of field of the camera is closely related to the image magnification. The depths of field at magnifications of 1:1 and 2-1/2:1 are 0.88 mm and 0.25 mm respectively, differing by almost a factor of 4 (see Appendix I). It is desired to have a depth of field at least as large as the drop diameter. In this photographic problem, it is difficult to simultaneously satisfy the various requirements as closely as would be desired because of the way in which these requirements interact. If the magnification is made small the depth of field increases. Since it is beneficial to have a large depth of field, this appears to be the proper method of attack. However, when small magnifications are employed, errors in interpreting the film become great. A compromise must be reached where each of these aspects, depth of field and magnification, are reasonably satisfied. In order to maximize the depth of field, the relative aperture of the lens is made as small as possible.

Illumination requirements are severely restrictive in the photography

of the drops. High intensity illumination must be employed to compensate for the very short exposure times. Because of the small apertures dictated by depth of field considerations, the illumination problem is intensified. The light sources employed in this experiment are high intensity photoflood lights.

Although the light sources can be placed at any horizontal position at the height of the test section, ranging from front lighting to back lighting only two conditions are considered: Side or back lighting. Positioning of the light will determine the relative brightness of the drops with respect to their background, When side lighting is employed the drop surface is bright with the background appearing dark. The difference in brightness on the film between the drop surface and the background is great enough so that it is easy to identify the drop surface. When backlighting is used, the drops appear grey against a light background. In this case distinguishing the surface of the drop from the background is more difficult. Although side lighting allows more precise determination of the position it also requires much greater illumination intensity than does back lighting. In both cases, proper illumination intensities must be empirically determined.

III. EQUIPMENT

The equipment developed for use in this study can be divided according to function into six components: 1) gas pre-mixing section, 2) main gas heater, 3) test section and entrance duct, 4) thermal blanket system, 5) injection system, and 6) photographic equipment. The integrated system is depicted in Fig. 1. Oxygen and nitrogen, the gases which constitute the combustion atmosphere for the droplets, are metered at room temperature into the main heater where they are heated to 500-900°C. From the main heater the gases are led through an exit manifold to the vertical entrance duct and then through the test section. Droplets are injected upward into the combustion atmosphere from beneath the vertical duct.

Because of the high temperatures and small mass flow rates of gas, an active insulation must be used to reduce heat losses in the neighborhood of the test section so that temperature drops through the test section can be kept to a minimum. The active thermal insulation system consists of a set of auxilliary ducts largely surrounding the entrance duct and test section through which heated air is circulated. This thermal gas blanket provides the hot metered combustion atmosphere with surroundings nearly at its own temperature and in this way reduces or eliminates temperature driving forces for heat transfer to the surroundings. There is also a passive insulation used around all of the heated sections except the test section.

A. Gas Premixing Section

Oxygen and nitrogen are metered by a pair of Brooks Sho-Rate Type 4-1355V flow meters with a maximum flow rate for air of 10,000 cc/min at 70°F at one atmosphere pressure, into a stainless steel tube 1 inch outside diameter and 18 inches long. A stainless steel coarse mesh screen serves

to mix the gases through turbulence that it creates. The gases then pass to the main heater.

B. Main Heater

The main heater consists of a heating unit rotating in a stainless steel shell. The heating unit, as shown in Fig. 2, consists of a cylindrical array of 48, 1/4 in. diameter by 7 in. long ceramic rods mounted between two end plates. Of the 48 ceramic rods 46 are wound with approximately 1.25 feet each of 28 gauge chromel wire of specific resistance 4.1Ω/feet. One rod is wound with about 3.7 feet of the resistance wire, and another is not wound and serves only to balance the unit. The geometrical arrangement of the ceramic rods can be seen in Fig. 3. The 47 electrically wound rods are divided into six groups of seven rods and one group of five rods. The rods making up each group are connected in series. The seven groups are connected in parallel. The group that contains 5 rods contains the rod that has the extra wire. The equivalent resistance of this arrangement is about 6.1Ω. The end plates of the heating element, of 310 S.S., are 5 in. in diameter 1/16 in. thick and are mounted 5-1/2 in. apart on a 1-3/8 in. 316 stainless steel shaft. The heating unit is mounted in a horizontal cylindrical shell 7 in. in diameter, 9 in. long and 0.025 in. thick, formed in two sections with an asbestos gasketed horizontal joint. The material of construction of this shell is also 310 S.S.

Figure 4 shows the arrangement of the main shaft of the heater. The main shaft not only mechanically supports the heating elements but also carries electrical current to the heating elements. To accomplish these functions the main shaft, as shown in Fig. 5, consists of an outer metal tube that is the load bearing member and a pair of co-linear inner metal tubes, insulated from the outer tube by a concentric ceramic cylinder, that provide electrical paths to either end of the heating element. The outer

tube of 316 stainless steel is 1-3/8 in. OD, 1-1/8 in. ID, and 30 in. long. The end plates on which the heating elements rest, are mounted on this shaft. Inside this tube is the 1-1/8 in. OD × 7/8 in. ID ceramic insulator. The inner tubes are of 321 stainless steel and fit inside the ceramic tube; they are 7 in. long, 7/8 in. OD, and 1/2 in. ID. About 1 in. from the outboard face of each heater end plate, 1/2 in. holes are drilled through both sides of the outer stainless steel shaft and the ceramic tube. Through each of these holes a 4 in. long by 3/8 in. diameter threaded stainless steel rod is screwed into the inner stainless steel tube. These rods do not contact either the outer stainless steel tube or the ceramic tube. Around those portions where the rods might contact the outer shaft, Sauereisen Electric Resistor Cement is packed. In this manner the main shaft is completely insulated from the heater circuit.

The electrical circuit for the main heater is shown in Fig. 5. Copper plugs are screwed into the outboard end of the inner stainless steel tubes, and copper rods 1/4 in. OD are in turn screwed into these plugs. The copper rods extend to within 2 in. of each outer end of the main shaft. Stranded copper wire, having an equivalent diameter of a 1/4 in. rod, is silver soldered to these copper rods and then soldered to another pair of copper plugs that fit partially inside of the ends of the ceramic tube. These latter copper plugs are held in place at the end of the shaft by three nylon screws that go through the stainless steel shaft, the ceramic, and into the copper plugs. The electrical current passes to the heating element in turn through the copper plug, the stranded copper wire, which serves to take up any differential thermal expansion of the materials, and the copper rod into the stainless steel inner tube. From there it flows up the 3/8 in. stainless steel rod and into the coiled heating elements. The current exits through a similar arrangement on the other side after passing through the heating coils.

Power is supplied to the rotating unit through graphite impregnated porous bronze brushes that contact the copper plugs at the ends of the shaft. A spring is used to maintain pressure of each brush on the copper plug as the unit rotates. Figure 6 shows the brush contacting the copper plug. An autotransformer, Variac Type W20M, supplies a maximum of 20 amps and 140 volts to the main heater circuit.

The entire rotating assembly is supported by two SKF Model SYH 106X Pillow bloc adjustable bearings located about 8-1/2 in. from the end plates. The rotating assembly is driven through a 4:1 speed reduction timing belt drive by a 1/15 horsepower electric motor whose speed is controlled through a Minirik Model SH-33 power control. The maximum speed of the motor is 5500 RPM; therefore, the heating element has a maximum rotational speed of about 1400 RPM.

C. Test Section and Entrance Duct

As mentioned earlier, the test section is that part of the equipment where the burning or evaporating droplets are supported and photographed, and the entrance duct is the section through which the combustion atmosphere gases flow on their way to the test section.

The test section is constructed of flat Vycor glass plates 1/4 in. thick. As shown in Fig. 7, it has three channels through which gas can flow. The two channels through which the thermal blanket gas flows are incorporated in the diverging walls, each of which is made of two parallel pieces of glass, in between which insulating gas flows. Two pieces of glass fixed perpendicular to the diverging walls serve along with the diverging walls to enclose the combustion atmosphere on four sides. This is shown in Fig. 8. The separation of the diverging walls at the bottom of the test section is fixed at 4 mm. The separation at the top of the section is adjustable, the

maximum separation obtainable being 2 cm. The test section is approximately 4 cm wide.

The entrance duct as seen in Fig. 9 also has three channels for gas flow. The two outer channels carry the thermally insulating gas whereas the central channel carries the metered combustion atmosphere. The entrance duct is 35 cm long with a rectangular cross section in which the metered gas flows tapering from 2 cm × 4 cm at the bottom to 0.4 cm × 4 cm at the top. An additional section with parallel walls is available for increasing the overall length to about 40 cm. The material of construction is 310 stainless steel, which has a continuous operating temperature of up to 1100°C[18] in an oxidizing atmosphere.

D. Thermal Insulating System

Salabarria designed and described the shell of the reheater, the blower, and the duct work employed in the thermal blanket system in his earlier work.[16] The shell of the reheater is a long rectangular parallelopiped with a removable top section. The shell measured 11-7/8 in. × 1-1/2 in. × 2-1/2 in. The heating element of the reheater has been revised to three 15.4 foot coils of 21 gauge chromel wire connected in parallel. Each of the three coils is arranged uniformly in a zig-zag fashion within the shell of the heater, and the coils are supported at each change of direction by ceramic stand-off insulators. The approximate overall resistance of the unit is 11.7Ω. Power is supplied to the reheater by a Variable Autotransformer, Powerstat Type 146, with a maximum output of 140 volts and 30 amps.

Air is circulated through the closed circuit of the thermal blanket system by a centrifugal blower located upstream of the heater. The blower is driven by a 1/8 horsepower Bodine motor whose speed can be varied from about 1000 to 5000 RPM by a Cole Carmer SCR Voltage Controller Model 2600.

From the heater the air flows through the two outside channels of the entrance duct where the heated air serves to actively insulate the center section which carries the metered combustion atmosphere gases. This air then flows through the two diverging walls of the test section and is collected in an overhead hood and returned to the blower.

To further reduce heat losses, heating tapes are wrapped around the exterior of the ductwork; one around the duct between the main heater and the vertical column, and the other around the column. These heating tapes,* have a maximum output of 576 watts at temperatures of up to 1600°F. The voltage to the tapes is regulated by two Powerstat variable transformers Model 3PN1168.

E. Injector System

The basic design for the injector is depicted in Fig. 10, with the actual injector appearing in Fig. 11. The injector is a syringe type device whose cylinder is 1/2 cm in diameter for the lower 15 cm and 0.05 cm in diameter for the 6 cm nearest the nozzle. The nozzle, which is fixed at the end of the cylinder, is a cylindrical piece of stainless steel approximately 1/4 cm thick and 1 cm in diameter with an orifice drilled in the center. On the outboard side of the plate the wall of the hole is beveled at a 30° angle for 0.20 cm. Two such nozzles are available, one with an orifice of 0.025 cm in diameter and the other 0.038 cm in diameter. The nozzle is held in place at the end of the injector cylinder by a threaded collar, and to avoid leakage a teflon washer is used under the nozzle. The stainless steel injector plunger which is 0.45 cm in diameter and 15 cm long has a teflon band 1 cm long around the circumference of the plunger 1/2 cm from the top of the plunger which serves to

* Briskeat Samox Fiber Insulated Flexible heating tapes 1/2 in.×8 ft.

insure a good seal between the plunger and the cylinder wall. The injector plunger operates in the lower part of the cylinder. Fuel is stored in the cylinder and is forced out through the orifice by the motion of the plunger. The injector is surrounded by a cylindrical cooling jacket in which cooling water flows up a tube to the nozzle end of the injector. The cooling water then flows down the outside of the cylinder and out at the bottom of the jacket. This prevents appreciable vaporization of the fuel in the cylinder. The entire injector assembly is 21 cm long and 2 cm in diameter.

The unit is mounted pointing vertically upward with the nozzle positioned in the lower wall of the 90° bend in the main duct. It is held in place by twist-lock joints which also serve to align the injector with the entrance duct and test section.

F. Photographic Equipment

Photographs of the burning droplets in the test section are taken by a Fastax (Model WF17) 16 mm high speed motion picture camera. The camera is mounted on a variable height support block that slides on a lathe bed for adjustment of focus of the lenses on the test section. The lathe bed is supported by a heavy duty Uni-Strut structure.

The camera is capable of taking several thousand frames per second, but is most often used in this study at 1000 frames per second. It is equipped with a timing light which can record marks on the side of the film for timing reference. The timing light is operated at 1000 cps by 200 volt square wave pulses produced in a Hewlett-Packard Pulse Generator Model 214A. A Fastax-Raptar No. D51935 lens with focal length of 101.1 mm is used with extension tubes to vary the magnification from 1:1 to 2-1/2:1; the extension tubes vary in length from about 1-1/2 in. to 4 in. The film

used is DuPont 931A Rapid Reversal Panchromatic 16 mm high speed photographic film with resolution of 100 lines per mm.

High intensity lighting is provided by a high illumination photo flood lamp, Fastax Fastline WF322, with an adjustable parabolic mirror. The lights are General Electric Projection Lamp Model DRS with a maximum power of 1000 watts. The high intensity light from this source is uneven at short distances, because of the images formed of the filaments of the bulb by the parabolic mirror, and therefore a piece of ground glass is placed between the lamp and the test section as a diffuser. An example of the positioning of the camera and light source with respect to the test section is shown in Fig. 12.

G. Insulation and Temperature Sensing

In order to reduce heat losses, the heated equipment is insulated (Fiberfrax fibrous ceramic insulation capable of withstanding temperatures up to 2300°F.) The thermal conductivity of this insulation is about 0.1 BTU/hr. ft. °F in the temperature range that it is employed. The insulation is supported around the apparatus by an aluminum container, which is constructed so that a minimum thickness of six inches of insulation surrounds the heated equipment.

Temperature sensing of various parts of the equipment is accomplished by use of Pt-10% Rh-Pt thermocouples using wire of 0.02 in. diameter. The thermocouple leads are connected at a terminal strip exterior to the insulation, which serves as a room temperature cold junction. From the terminal strip the leads are connected to a continuous recording Leeds and Northrup Speedomax H Azar multipoint recorder which records the potentials of the thermocouples.

IV. PROCEDURE

The measurement of droplet burning rates can be divided into several distinct parts: equipment preparation, calibration, photography of burning or evaporating drops, and analysis of the photographic record.

Preparation of the equipment before an experimental run is made is a critical aspect of the work. The walls of the test section are first cleaned with tri-chloroethylene and then set to a desired separation at the top of the diverging walls. Next the photographic equipment must be calibrated and properly positioned before the apparatus is brought up to operating temperature. Magnification requirements determine the lens to be used and the distance from the test section at which the lens must be located. The camera is focused on a piece of thin wire which is suspended with its end on the center line of the test section, where the gas velocity will be a maximum. Coarse focusing adjustment is achieved by sliding the camera mount on the lathe bed, and fine focusing is realized by adjusting the lens. While the equipment is still cold, the light source is placed on the side of the test section opposite the camera. It is positioned so that the image of the lamp filament is focused by the parabolic mirror on as small an area of the ground glass as possible.

The power supply to the camera is adjusted to a voltage which corresponds to the nominal frame speed desired in the experimental runs. If the camera is to be operated at a nominal 1000 frames per second, there is a period of acceleration where the frame speed increases from zero to 1000 frames per second. The power supply is not altered throughout the experiment so that the nominal frame rate is the same for all cases.

To calibrate the object to image magnification and the local variation of this magnification over the field of view of the camera, pictures

must be taken of objects of known size. The objects used here are glass beads approximately 1000μ in diameter, the beads have been measured with a comparator microscope so that their diameters are known. Two beads are glued to a piece of fine wire, about 300μ in diameter, so that most of each bead is visible and distinguishable from the wire. With the camera prepared for operation and the photoflood light properly adjusted, the camera is started and calibration pictures are taken as the beads and wire are moved to various positions in the field of view of the camera. In this manner, a photographic record is obtained that is sufficient to calibrate the object to image relation over the field of view of the camera.

In all subsequent photography, a timing reference is required. For this purpose the pulse generator is attached to the timing marker assembly of the camera. The pulse generator is set to provide square waves at 1000 cycles per second, 200 volts and 150μ second pulse widths.

The thermocouples, the thermocouple probe which is used to measure the temperature of any position in the test section, and the injection system are all checked to assure that they are functional. The electrical resistance of each heater is then checked for any short or open circuits in the heaters. The temperature recording device is started and a log is kept of any changes in applied currents, motor speeds, and air flow rates.

Heating the equipment to the desired temperatures, 500°-900°C is the most time consuming step of the running of the experiment. Before any power is turned on, all cooling systems are started except the cooling of the injector, which is not fixed into position until droplets are to be injected. Air flow through the test section is set at the desired rate, and the main heater rotor and reheater fan are adjusted to the desired speeds, 700 RPM for the main heater rotor, and 5000 RPM

for the reheater fan. Power is first applied to the heating tapes, which are allowed to heat the system until the air in the test section reaches about 450°C as determined with the aid of the thermocouple probe. Power is then slowly increased to both the main heater and the reheater. Usually, the incremental changes in current to either heater do not exceed 2 amperes because of the chance of thermal shock to the equipment. Once the current in the heating elements of the main heater reaches 5 amperes, increases in current are in 1/2 ampere increments every half hour. Under these conditions the apparatus is brought up to the desired temperature. While the equipment is being heated, the lens is removed from the camera so that it will not sustain any harm from being in close proximity to the hot test section for a long period of time.

The currents necessary to bring the equipment to the desired temperature within a reasonable amount of time will be greater than the currents necessary to sustain the equipment at that temperature. Consequently, when the apparatus approaches the desired temperature, the current to both heaters must be reduced until the steady state is reached. To insure stabilized conditions the equipment is allowed to remain at the desired conditions for about half an hour.

Once the equipment has reached and is stabilized at the desired temperature, the injection cylinder is filled with about 5 cc of n-heptane, with a hypodermic syringe. The aluminum cover that seals the slot where the injector is to be positioned is removed and the injector is inserted. The injector is tested two or three times by manually operating the plunger so that a few droplets reach the test section. The camera is loaded with film, the lens is replaced in the camera, the pulse generator is started, and the photoflood lights are turned on.

When the camera is operated at about 1000 frames per second, it takes about 1/2 second for the camera to accelerate from rest to the desired speed; it takes about the same amount of time for droplets formed by the injector to reach the test section. The camera is started, and at the same time the plunger of the injector is manually moved short distances two or three times so that droplets can be injected into the test section more than once during the running time of the film. Operating at 1000 frames per second the camera uses the 100 foot roll of film in about three seconds and then the camera motor automatically shuts off.

Whenever the equipment is to remain at elevated temperatures for over 15 minutes without any pictures being taken, as in the case of changing the temperature of the apparatus, the injector is removed and the aluminum cap is replaced over the injector slot.

Following completion of the experimental measurements, power to the heaters is slowly reduced, and power to the heating tapes is shut off. With the main heater rotor and the reheater fan still operating and with the coolants still flowing, the equipment is allowed to return to room temperature.

The film from the experimental run is developed, and viewed with the aid of a 16 mm projector. The photograph of the beads are viewed first to make sure that the beads traversed the field of view of the camera. If they did not, another calibration run can be made since the camera and the test section remain in the same positions they occupied during the experimental runs. The film records of the evaporating or burning droplets are next examined for suitable events, a suitable event being 30 or more frames of a single stabilized spherical droplet. These events are marked, so that when measurements are to be taken from the film the

event can easily be located. When all of the film from an experimental series has been examined, measurements of droplets involved in the chosen events are taken with the aid of a Vanguard Motion analyzer. The analyzer is equipped with calibrated horizontal and vertical moveable wire grids that are used to measure distances on the screen. The photographs of the beads are measured first so that the magnification throughout the field of view of the camera can be calculated from the known size of the beads. Once the magnification as a function of position is known, the diameter and position of these droplets which appear for the desired number of frames is measured. The time interval between successive frames is determined from the distance between corresponding parts of successive timing marks (which is known to represent a 1/1000 of a second time interval) and the distance between corresponding parts of successive frames. In this manner data can be obtained in the form of a record of drop diameter and velocity as a function of time.

V. RESULTS

The effect of drop diameter, convection and temperature on the burning behavior of individual n-heptane droplets can be examined in the measurements made in this investigation. The data used were obtained from the photographic records of burning droplets as described in the previous chapter. These records cover the burning histories of droplets, or "events", at relative velocities from 30 to 90 cm/s, temperatures from 550°C to 700°C, and drop diameters ranging from 100μ to 500μ. A representative photographic record for a particular event can be seen in Fig. 13. From this type of pictorial record the diameter and velocity of each individual droplet can be determined as a function of time. In most events the droplet under investigation appeared spherical, but distortion from the spherical shape was evident for droplets of diameter greater than 500μ. Distortion of these droplets was caused by form drag and by frictional forces exerted by the gas moving tangential to the droplet at the droplet surface. For cases where the drop diameters, measured along axes at right angles to each other, as described in the previous chapter, were different by 5% no attempt to obtain data from the photographs was made.

Even though drops appeared to be burning in the test section when the photographs were being taken, no evidence of a flame front exists in the photographs. This is attributed to the high intensity back illumination employed compared to the relatively low luminosity of the n-heptane flame.

The theoretical study of burning rates of individual droplets by other investigators leads to the conclusion that the rate of change of

the square of the diameter of a burning droplet should be a linear function of time.[1,3,8] This result is derived under the assumption of fast chemical reaction, and constant physical properties as a function of temperature. The negative constant of proportionality between the square of the diameter and time is termed the burning rate coefficient. Burning rate coefficients were calculated in this work by a linear regression analysis of the square of droplet diameter on time for each event, which provided the value of the coefficient and the standard deviation of that value. All events which produced standard deviations of the burning rate coefficient greater than 5% of the coefficient were rejected. Figure 14 represents the relationship between the square of the diameter and time for the droplet of Fig. 13. The slope of this line gives a coefficient of 0.0128 cm^2/s with a standard deviation of 2%. The relative velocity of a droplet as a function of time is determined from the known velocity of the gas at the point in question in the test section and the apparent velocity of the drops in successive frames of the film. The gas velocity is determined from the measured volumetric flow rate of the gas, the geometry of the test section, and the temperature of the test section. The relative velocity of the droplet in Fig. 13 appears as a function of time in Fig. 15.

When the photographic records obtained in this study were screened, as described above, fifteen events remained for which burning rate coefficients were established. These events cover a range of temperature from 550°C to 700°C, of relative velocity from 30 to 90 cm/s, and of drop diameters from initial diameters of 410μ down to final diameters of 132μ. They are summarized in Table I.

From the theoretical work of Godsave,[1] Spalding,[2] Goldsmith and Penner,[3] and others, it is expected that drop diameter will have no effect on burning rate coefficients for burning under conditions of spherical symmetry, constant physical properties, and an infinitely fast reaction at the flame front. This should be true for the size range where drops are small enough to maintain their spherical shape (drop diameter less than 1000μ) and at the same time are large enough so that surface forces can be neglected (drop diameter greater than 5μ). The droplets in this work, diameters from 132μ to 410μ, from which burning rate coefficients were calculated, were approximately spherical. Unlike the droplets considered in the theoretical work that has been mentioned, the droplets investigated in this experiment were subjected to forced convective conditions. However, even in the presence of convective conditions no consistent dependence of burning rate coefficient on drop diameter was noticed. This lack of dependence of burning rate coefficient on drop diameter can be seen in the data of Table I. The burning rate coefficients at either 620°C or 700°C, the temperatures at which more than one value of the burning rate coefficient was obtained, show no tendency toward increase or decrease with increasing drop diameter.

Burning droplets studied in this work were falling near their terminal velocity under the influence of gravity. It appears under these conditions that convection has no appreciable effect for the burning rate coefficients determined experimentally in this work. The influence of convection on the evaporation rate for droplets evaporating into a hot environment of their own vapor has been studied theoretically by Wijffels,[17] and the effect of slow viscous flow on the burning of a droplet has been analyzed

by Fendell, Sprankle, and Dodson.[21] It is concluded in Wijffel's work that the effect of convection can be characterized by the dimensionless ratio of the free stream convective velocity to the velocity of the evaporating material at the surface of the droplet, termed the "evaporation velocity" and that the effect of convection for Reynold's numbers less than one is second order. The convective conditions as existed in this work were all characterized by Reynold's numbers smaller than one so that Wijffels' conclusions should be applicable. The evaporation velocity at the surface of the drop is proportional to the inverse of the diameter of the drop, so that the size of the drop will effect the evaporation velocity, and therefore the ratio of the convective to evaporative velocities. However, it has already been mentioned that the drop size did not appear to have an effect on the burning rate coefficient. The reason for the apparent lack of a noticeable effect of convection on burning rate coefficient may be because of the small effect on evaporation rates that convection does have. If the effect of convection is on the same order of magnitude as the standard deviation of the burning rate coefficients at a given temperature and convective condition, 8%, then the effect of convection will be unnoticed, as in the present case.

When the photographic records of individual events are analyzed, very slight variations in evaporation rate which might be attributed to convection can be noticed. However, because of the small magnitude of this effect and the unreliability of a single event, no firm conclusion can be drawn. Such is the case for the event depicted by Figs. 14 and 15. From time 0 to 10×10^{-3} sec, as reported in Fig. 15, the relative velocity of the drop apparently decreased from 70 cm/s to 35.5 cm/s.

The relative velocity of the drop remained near 35.5 cm/s until time 27×10^{-3}s. From time 27×10^{-3}s to time 34×10^{-3}s the relative velocity decreased from 35.5 cm/s to 30 cm/s. Comparison of these velocity changes to the record of square of diameter versus time for the same event, Fig. 14, shows a possible relationship between velocity and burning rate. The first 10×10^{-3} seconds, where the velocity was highest, exhibited a slightly greater evaporation rate than the remainder of the curve. The increase in the evaporation rate in this region is small enough, however, to be considered within the standard deviation of the slope of the curve, 2%. From time 27×10^{-3}s to time 34×10^{-3}s where the velocity was decreasing from 35.5 cm/s to 30 cm/s no effect on the burning rate was noticed. The effect of convection on burning rate coefficient as exhibited in Figs. 14 and 15 tend to confirm Wijffels' conclusions that convection has a second order effect.

Another aspect of convection that is noticeable in the data obtained in this work, is the effect of burning and evaporation on the terminal velocity of a droplet. According to simplified theoretical analysis of the process the large radial velocity of the evaporating material at the surface of the droplet should cause the burning droplet to attain a larger terminal velocity than a non-evaporating drop under the same circumstances.[19] This phenomenon has been noticed experimentally for individual droplets by Bolt and Saad,[11] and also for sprays of many droplets by Ingebo.[19] The radial velocity at the surface of the droplet tends to reduce the drag coefficient for the droplet, leading to the higher velocity. Figure 16 shows a series of photographs of a burning droplet that has reached its terminal velocity. The relative velocity between this 140μ droplet and the gas is 35.5 cm/s. For a non-evaporating

n-heptane droplet of the same size and subject to the same conditions the terminal velocity is calculated to be 26.3 cm/s (Appendix 3). The radial velocity at the surface of this droplet is 36.5 cm/s (Appendix 4). The ratio of experimentally determined and calculated (non-evaporating) values of terminal velocity for this burning droplet is comparable to results obtained by Bolt and Saad.[11] Under similar circumstances they obtain a ratio of 1.70 whereas the ratio determined in this work is 1.35.

The theoretical effect of temperature on burning rate coefficient for the non-convective case is most thoroughly analyzed by Goldsmith and Penner.[3] Their theoretical model, called the "diffusion theory", is based on assumptions of spherical symmetry, instantaneous chemical reaction at the flame front, and average values of physical properties over the range of temperatures existing in the gas. This theory agrees well with experimental results obtained by several investigators for droplets burned in surroundings near room temperature. A comparison between these burning rate coefficients and those from the diffusion theory can be found in Fig. 17 and Table II.

At elevated temperatures the diffusion theory mentioned above predicts a small rate of increase for the burning rate coefficient with temperature. Instead of this small temperature effect, the data of the present investigation show a large effect of temperature on burning rate coefficient under convective conditions. The average burning rate coefficients at the three temperatures investigated in this work were found to be:

T°C	K cm^2/s
550	0.0099
620	0.0115
700	0.0126

From these three values, it appears that the burning rate coefficient increases at the rate of 1.8×10^{-4} $cm^2/s°C$ in the temperature region 550°C to 700°C. The diffusion theory would predict an increase of only 1.5×10^{-6} $cm^2/s°C$ in the absence of convection. Furthermore, the simplified theoretical treatments of convection that were mentioned above do not predict any strongly temperature dependent convection effect.

The result obtained at 550°C in the present work is based on only one event. It might be suspected that the experimentally determined value of the burning rate coefficient at 550°C is in error. However, when the values of the burning rate coefficients are plotted as a function of the logarithm of the difference between the temperature of the environment and the boiling temperature of the drop (98°C) as suggested by the work of Goldsmith and Penner, all three points fall on a fairly straight line as seen in Fig. 17. Bolt and Saad[11] report a burning rate coefficient of 0.0195 cm^2/s for n-heptane at 815°C and at a relative velocity of about 215 cm/s (Appendix 6). This value is much larger than predicted by available combustion theory. However, when compared to the results of this work presented as a function of temperature in Fig. 17 it seems consistent with the temperature dependence found here. Moreover, in the only other study of burning rates at high environmental temperatures, Kobayasi[20] determined burning rate coefficients at 700°C and 800°C which also appear to have the large temperature dependence noted here. The results are included in Fig. 17; although they were measured under free convective conditions they correspond much more closely to the behavior found in this study than to the results available in the literature for combustion at low temperatures.

Although only a very few values have been measured for burning rate coefficients of n-heptane at environmental temperatures about 500°C, in this available data there appears a consistent pattern of significant increase of burning rate coefficient with temperature. The strong temperature dependence of the burning rate coefficient which appears in this work cannot be explained according to the available theoretical treatments of droplet combustion. It may indicate at elevated temperatures, about 500°C, that burning droplets are subject to phenomena that are not considered in the theoretical models to date. For instance, small rapid pulsations in the shape of the droplet might occur that lead to turbulence inside the flame envelope and thus to increase burning rate coefficients.

The only other work in addition to the present work and that of Bolt and Saad concerning convective burning of drops was carried out by Goldsmith[8] who, while working with 1500-1800μ diameter droplets at room temperature, determined the burning rate coefficient for n-heptane subject to three different convective velocities. The ratio of the convective to the evaporative velocities, which characterizes the effect of convection, for Goldsmith's work is a factor of two smaller than that for the work of this investigation. Because this ratio differs in these two studies and because Goldsmith's data are not in the same temperature range as this work no direct comparison between the two results should be made. However, the burning rate coefficients determined by Goldsmith are included in Table II.

Much more data are needed concerning burning rates of individual droplets, especially at elevated temperatures. As was expected, the results of this work indicated no effect of droplet diameter on burning rate coefficient. Convection appears to have a second order effect on

the rate of burning of droplets at elevated temperatures. The rate of increase of the burning rate coefficient with temperature found here was much greater than any that could be explained by present theories. However, the results of the other investigations conducted at elevated temperatures seem consistent with the slope of the burning rate coefficient as a function of temperature determined here. Much more might be said about the apparent rate of increase of the burning rate coefficient, if data were available at temperatures above 700°C.

VI. CONCLUSIONS

The value of the burning rate coefficient found for n-heptane at the lowest temperature investigated in this work, 550°C, agrees with the value of the coefficient calculated using simple theoretical models at that temperature, and with the room temperature coefficients determined experimentally by many investigators. However, the rate of increase of the burning rate coefficient with temperature was found here to be much greater than could be expected on the basis of present theories describing droplet combustion. This rapid increase in the coefficient over the temperature range of 550°C to 700°C appears to be consistent with the results of Bolt and Saad[11] and Kobayasi[20] who also made burning rate measurements, under forced and natural convective conditions respectively, for n-heptane at elevated temperatures. Many more burning rate measurements in this temperature range and at higher temperatures are needed in order to firmly establish the dependence of burning rate coefficients on temperature at high environmental temperatures and the effect of convection under these conditions. If the temperature effect on burning rate coefficient is as large as is suggested by this investigation, then it appears that phenomena that have not been considered in present combustion theories are significant at elevated temperatures and/or under forced convective conditions.

The influence on burning rate coefficient of both drop diameter and convection as determined in this work tend to agree with the theoretical and experimental findings of other investigators concerning these effects.[3,8,17] Drop diameter seemed to have no effect on the burning rate coefficient, for the diameters between 100μ and 500μ, studied here.

Also, convection had little or no effect on the burning rates measured for individual droplets in this work.

ACKNOWLEDGMENTS

The author would like to dedicate this thesis to William Blake.

This work was supported by the United States Atomic Energy Commission.

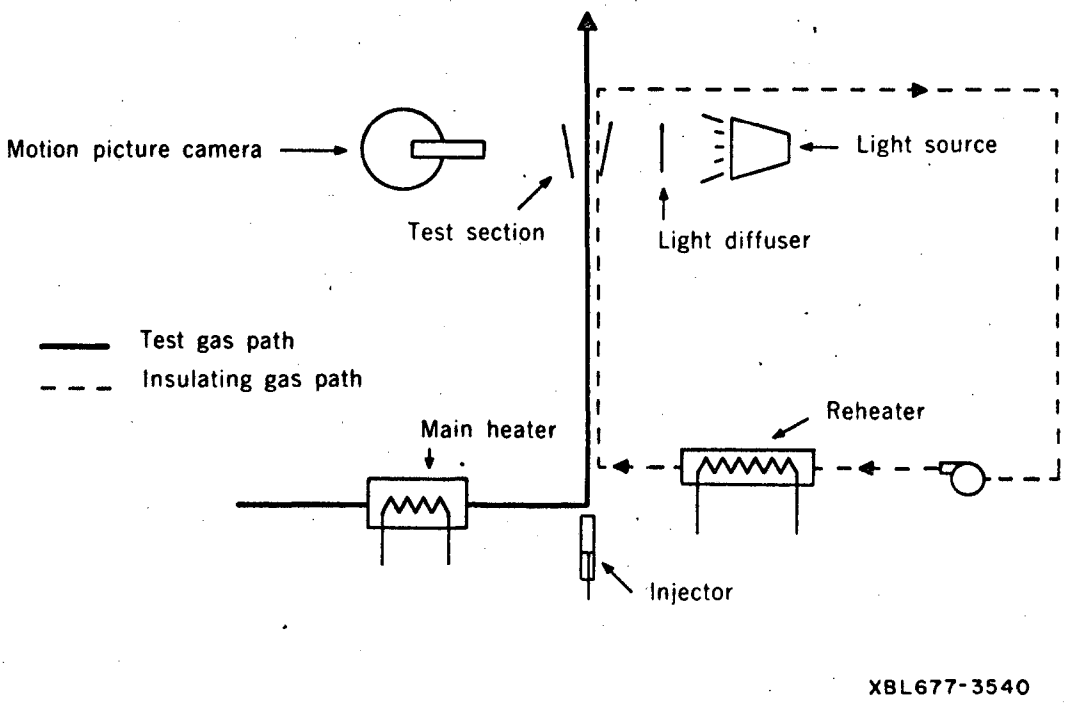

Fig. 1 Droplet combustion apparatus

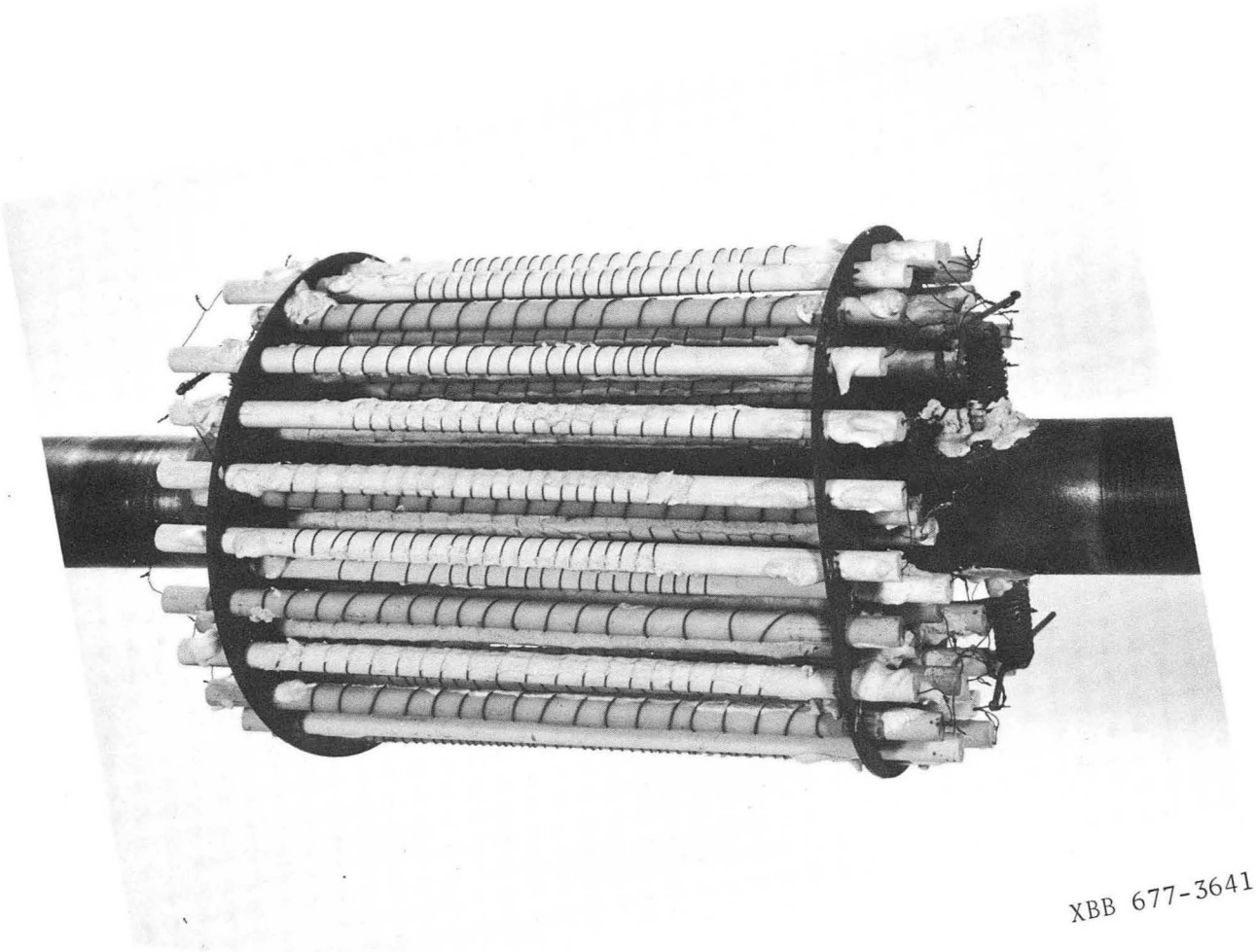

XBB 677-3641

Fig. 2 Main heater rotor

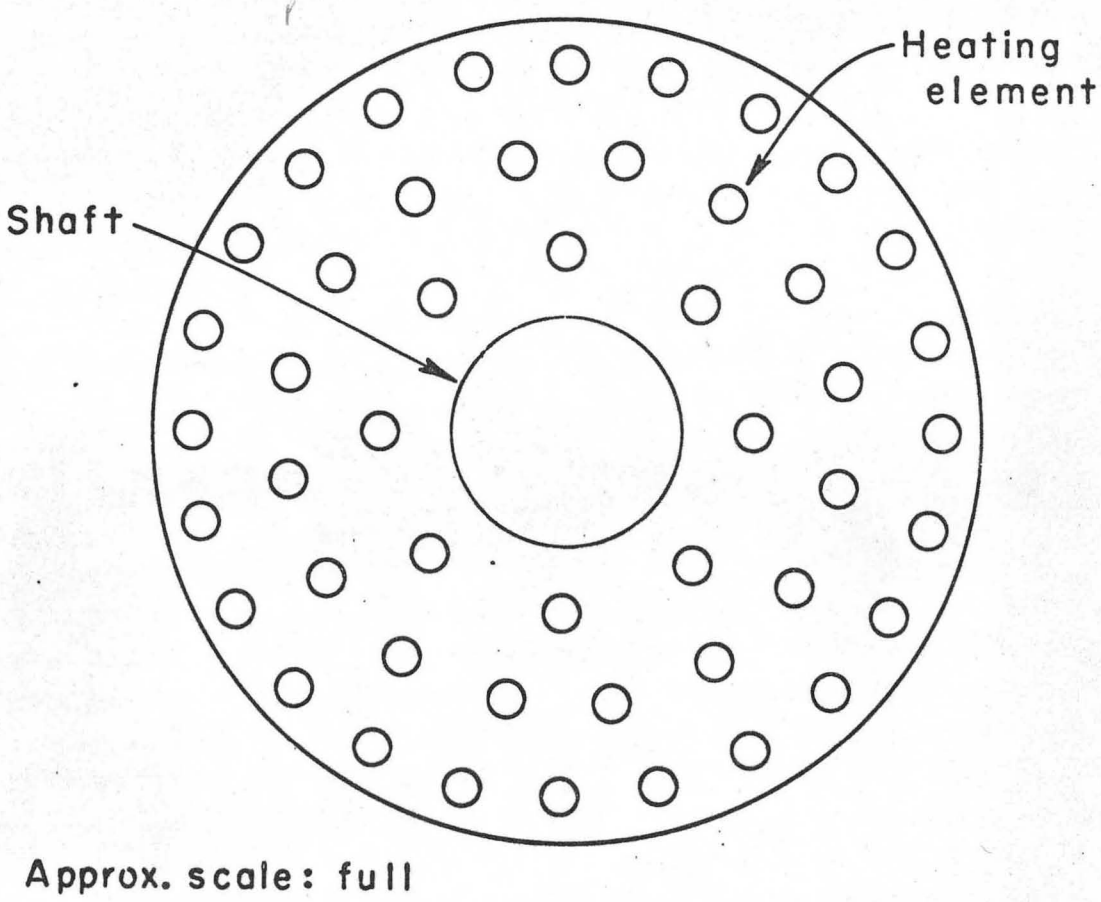

Fig. 3 Geometric arrangement of heating elements in rotor

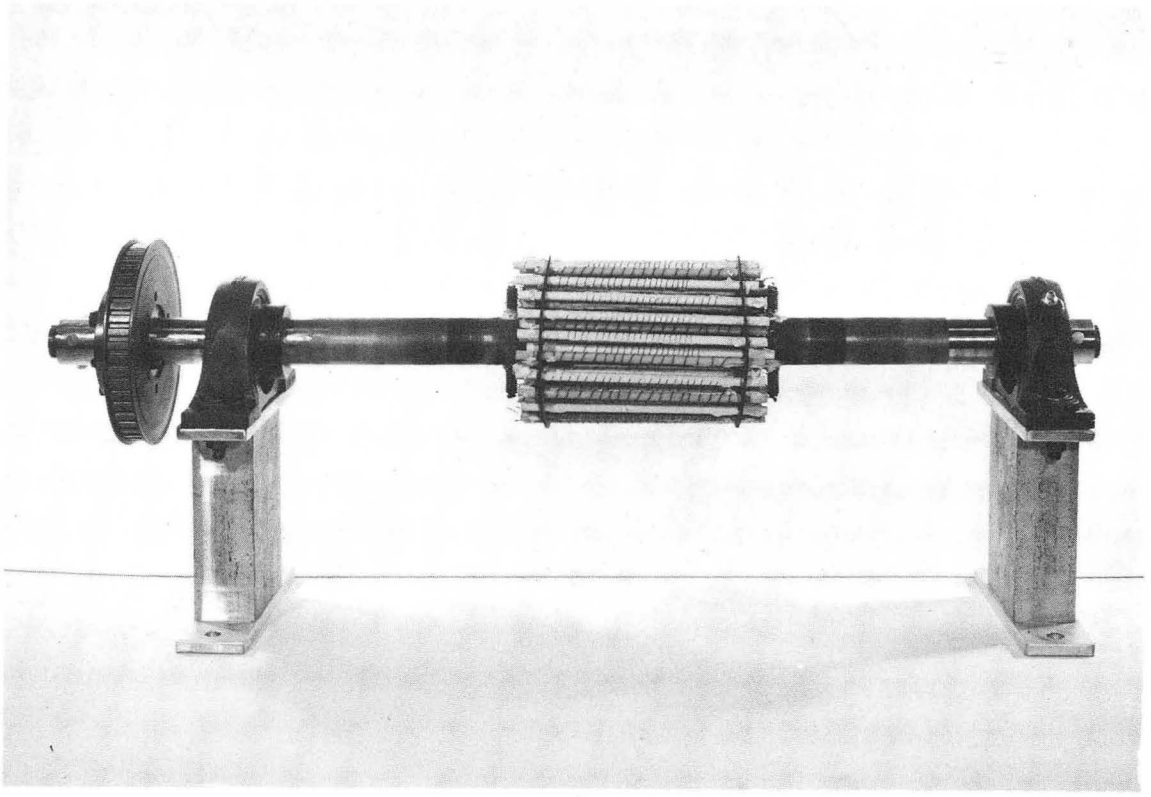

XBB 677-3639

Fig. 4 Main heater shift arrangement

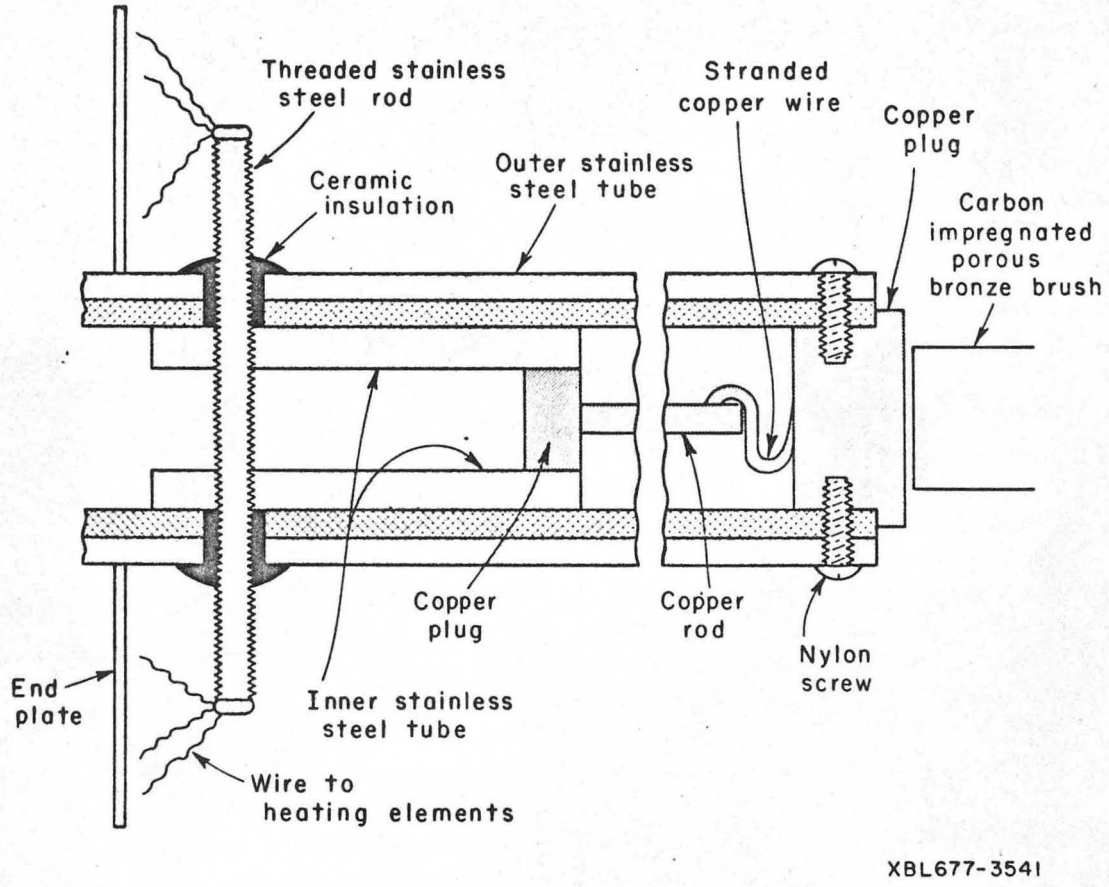

Fig. 5 Sectional drawing of main heater shaft

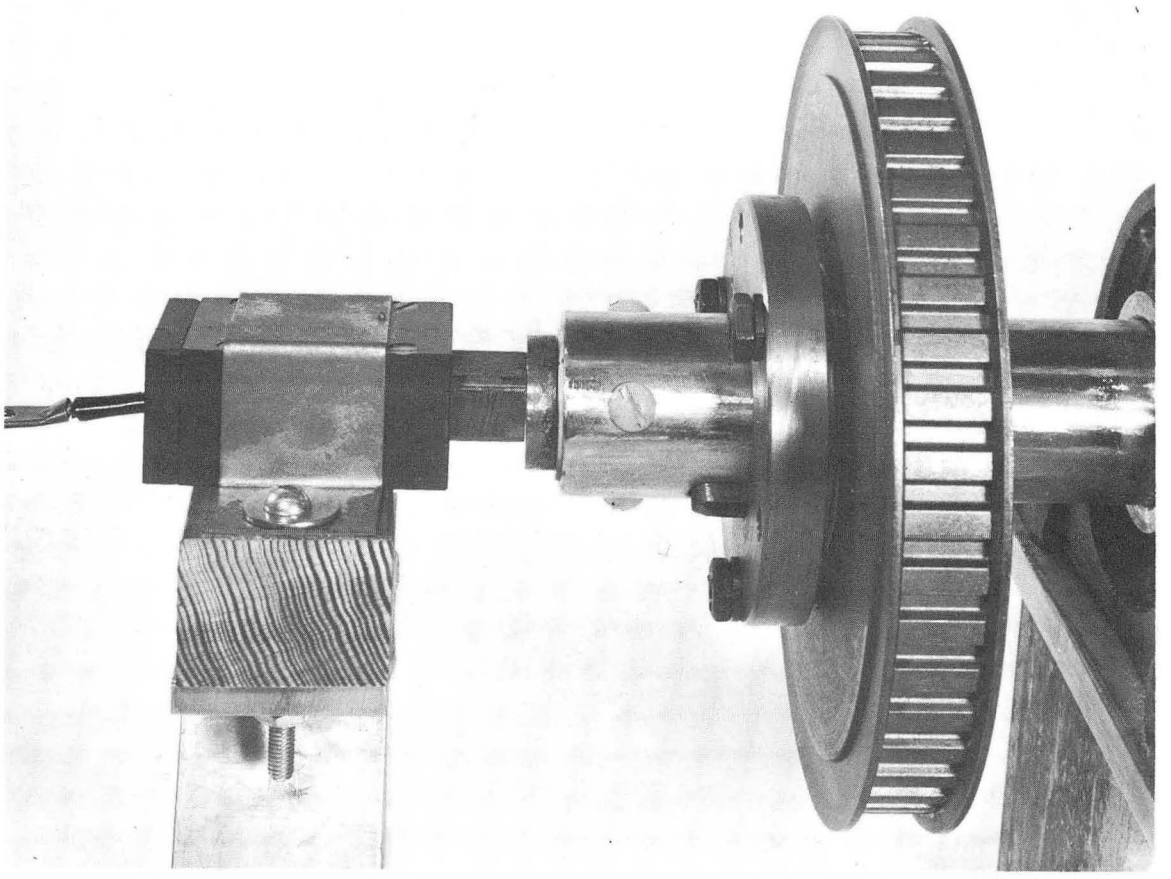

XBB 677-3640

Fig. 6 Main heater brush contact

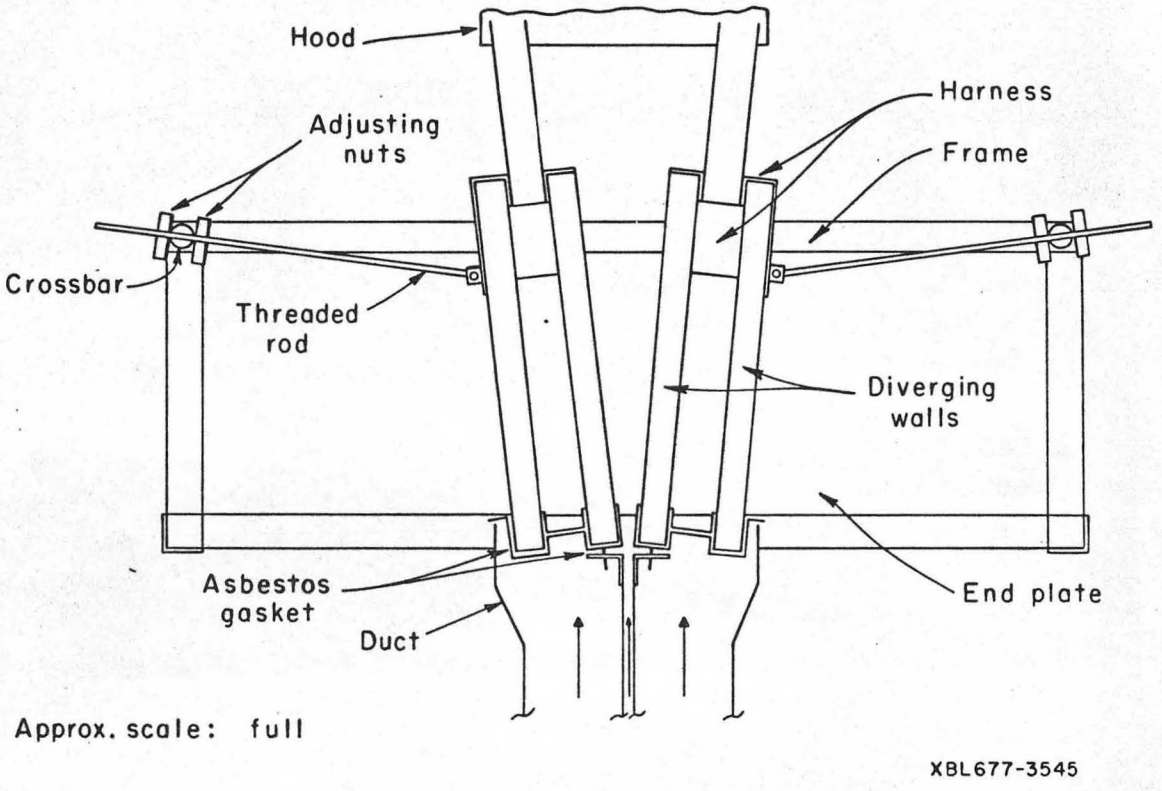

Fig. 7 Sectional drawing of test section

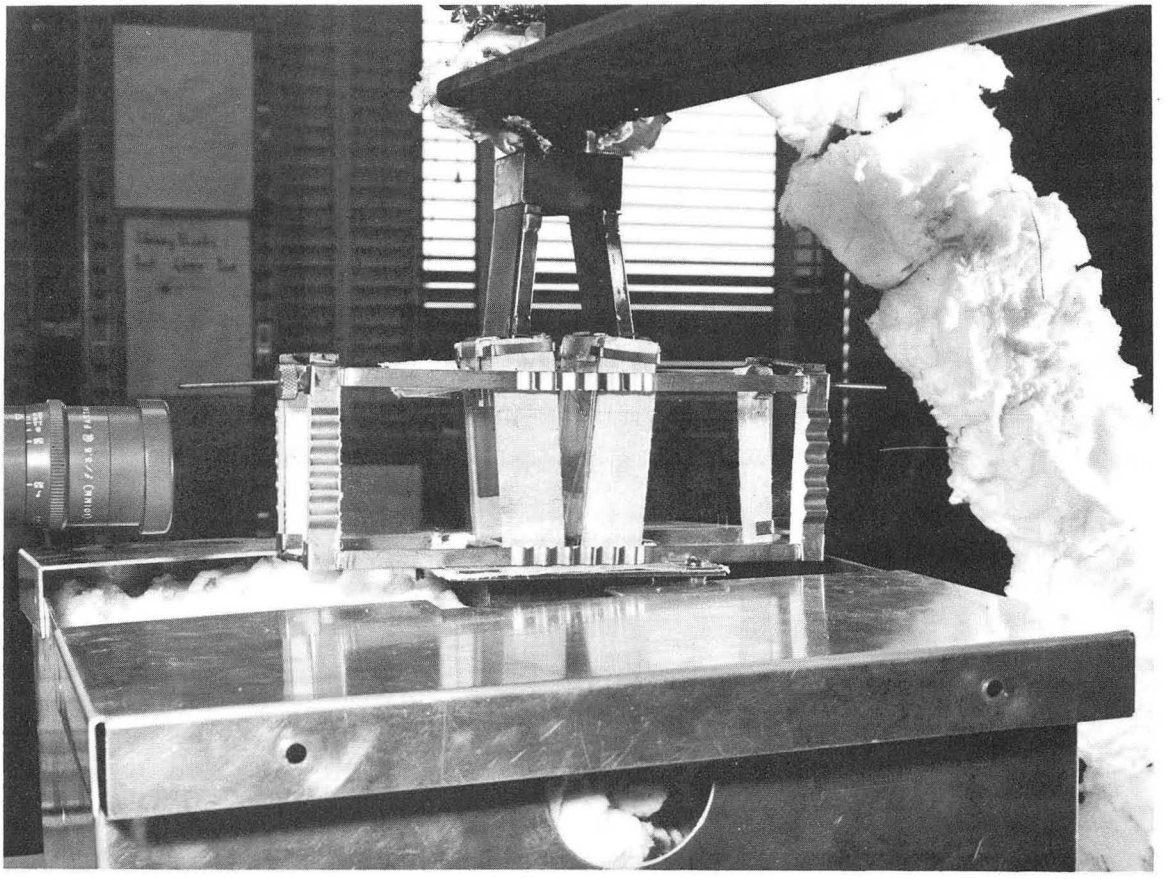

XBB 673-1361

Fig. 8 Test section

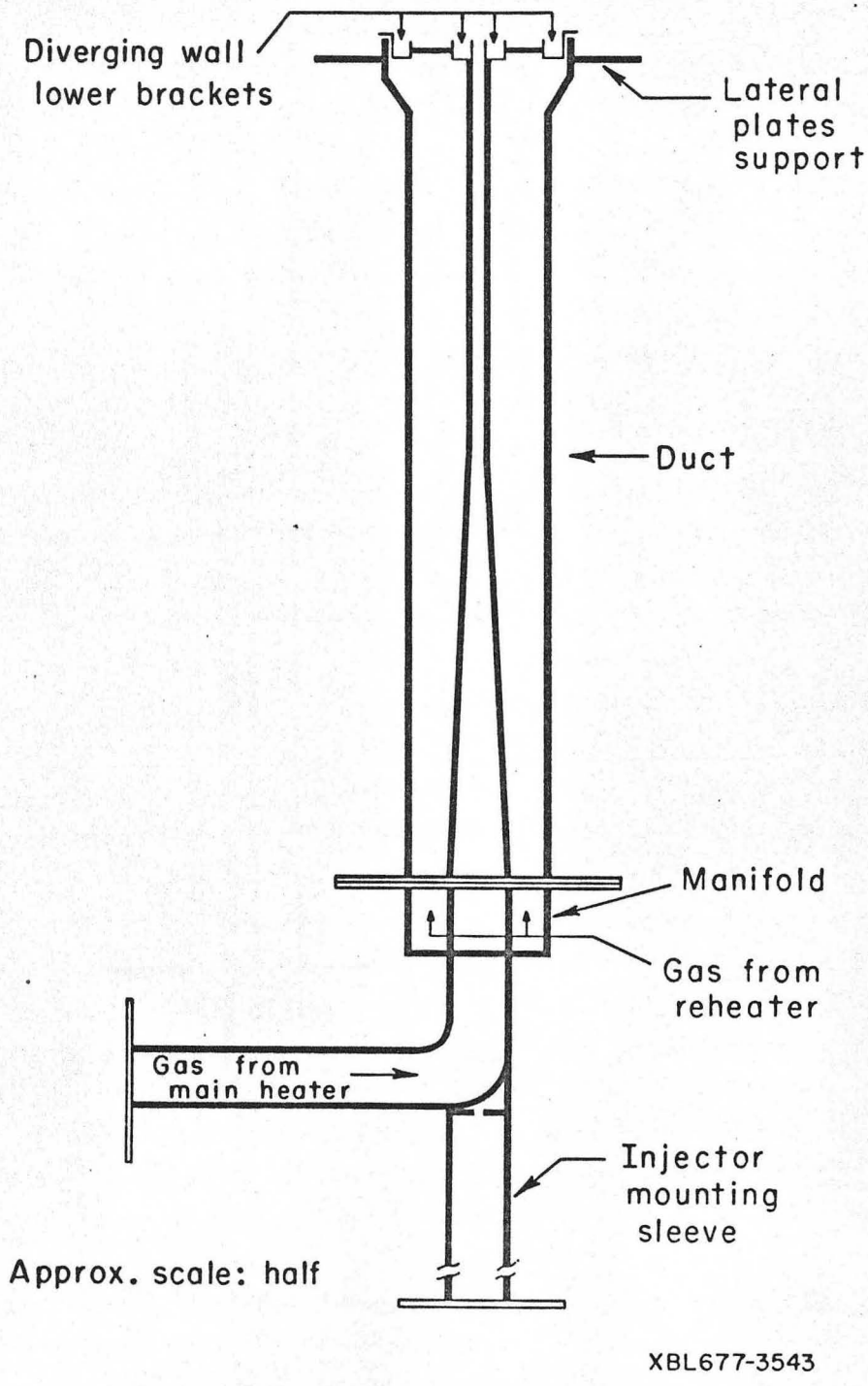

Fig. 9 Sectional drawing of duct and preceding section

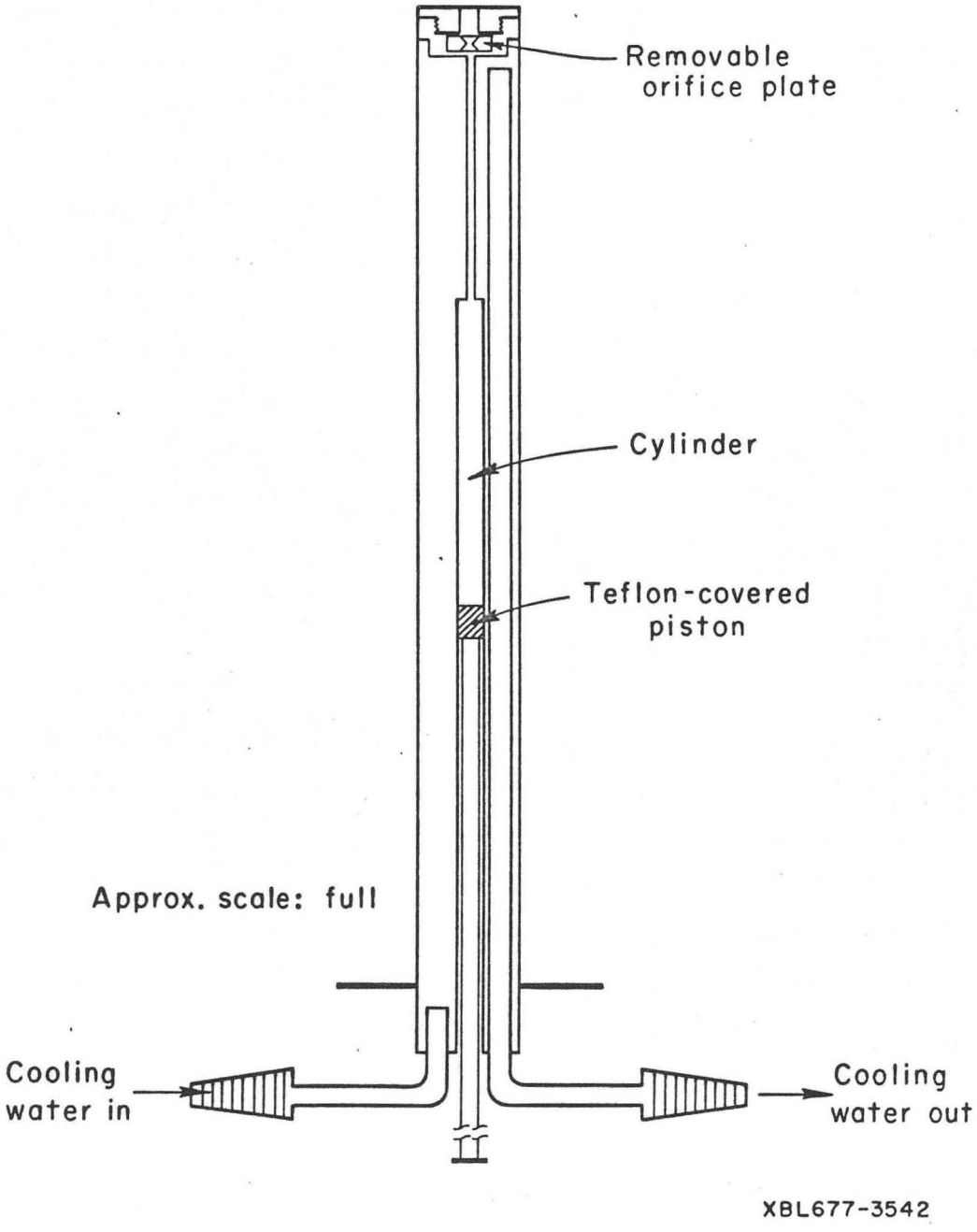

Fig. 10 Sectional drawing of injector

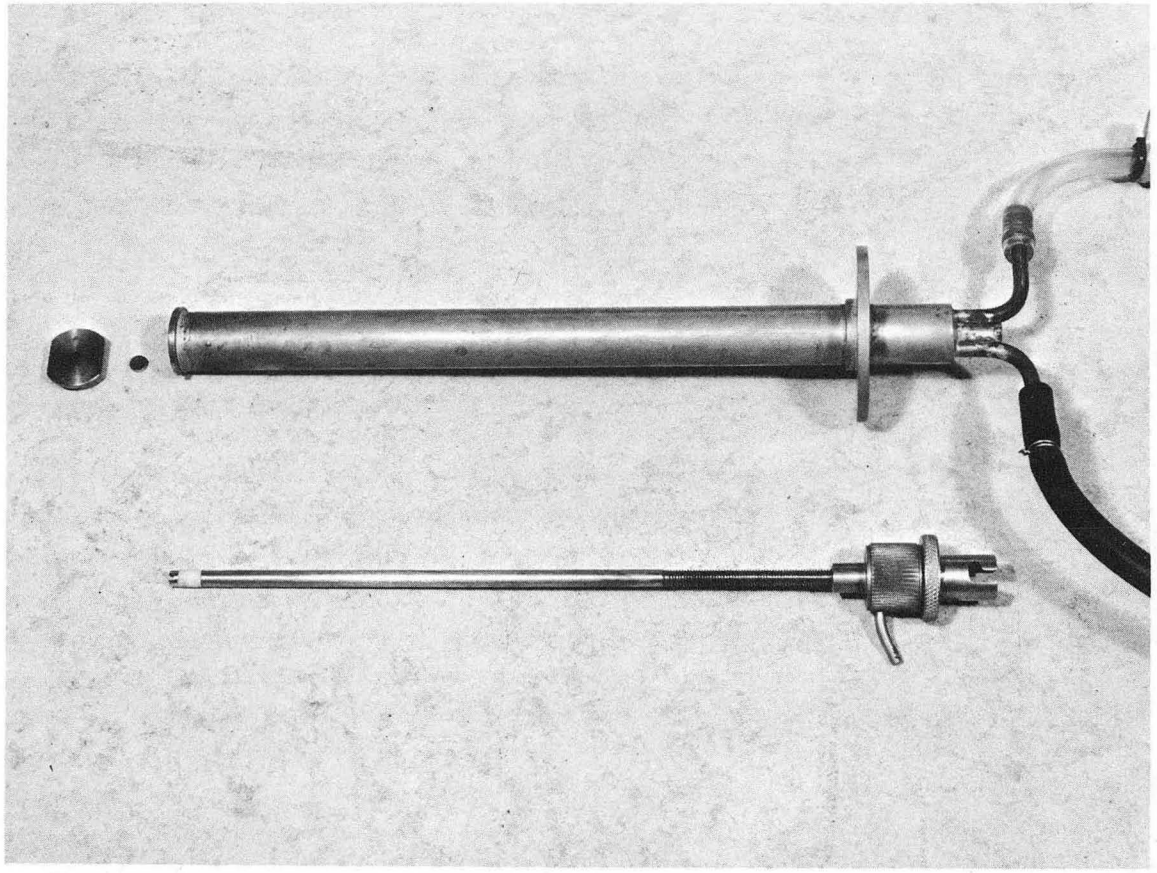

XBB 673-1360

Fig. 11 Injector assembly

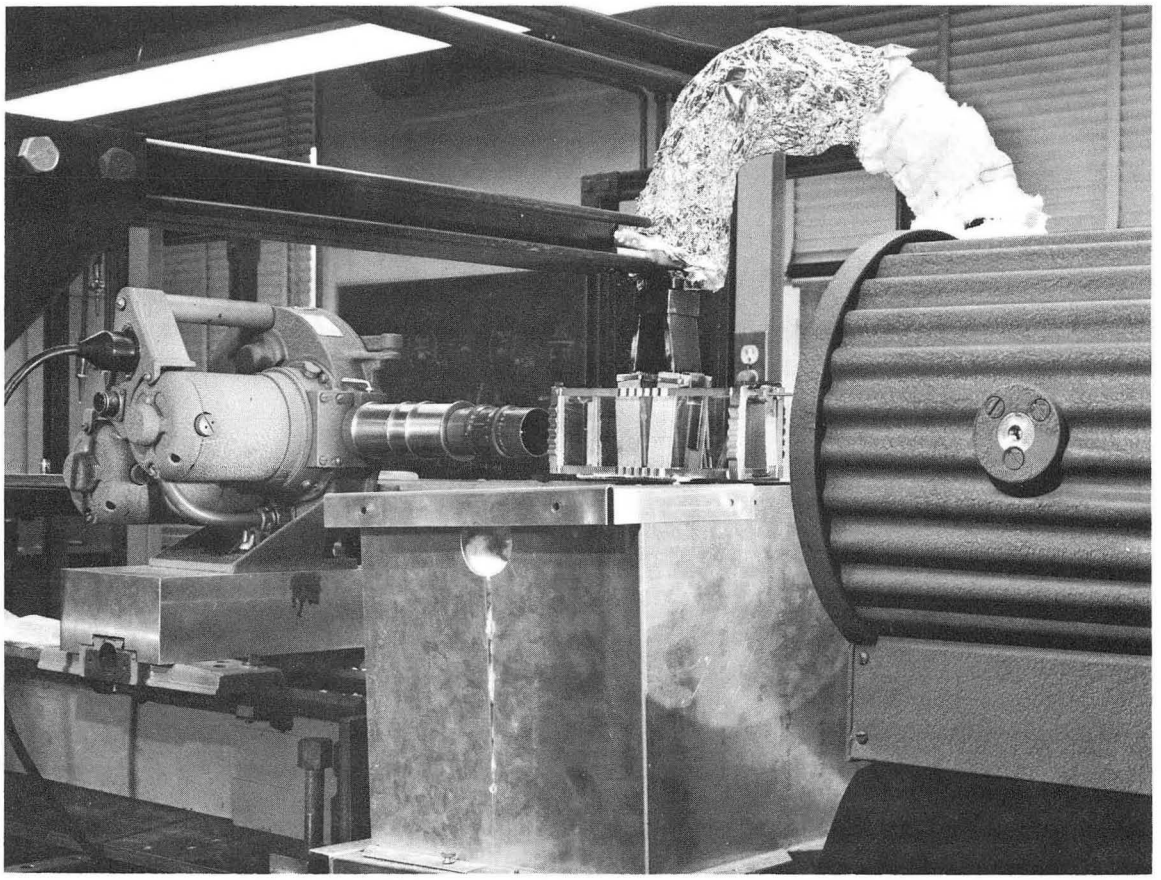

XBB 673-1362

Fig. 12 Lighting arrangement

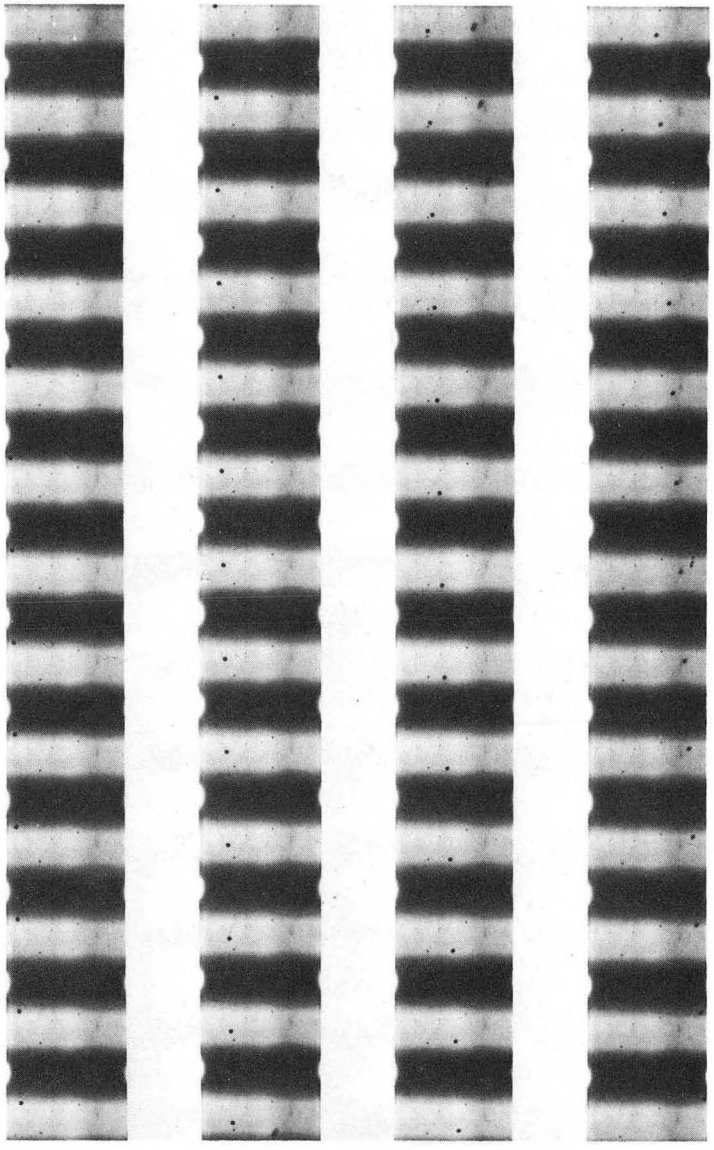

XBB 677-4148

Fig. 13 Droplet supported in air stream

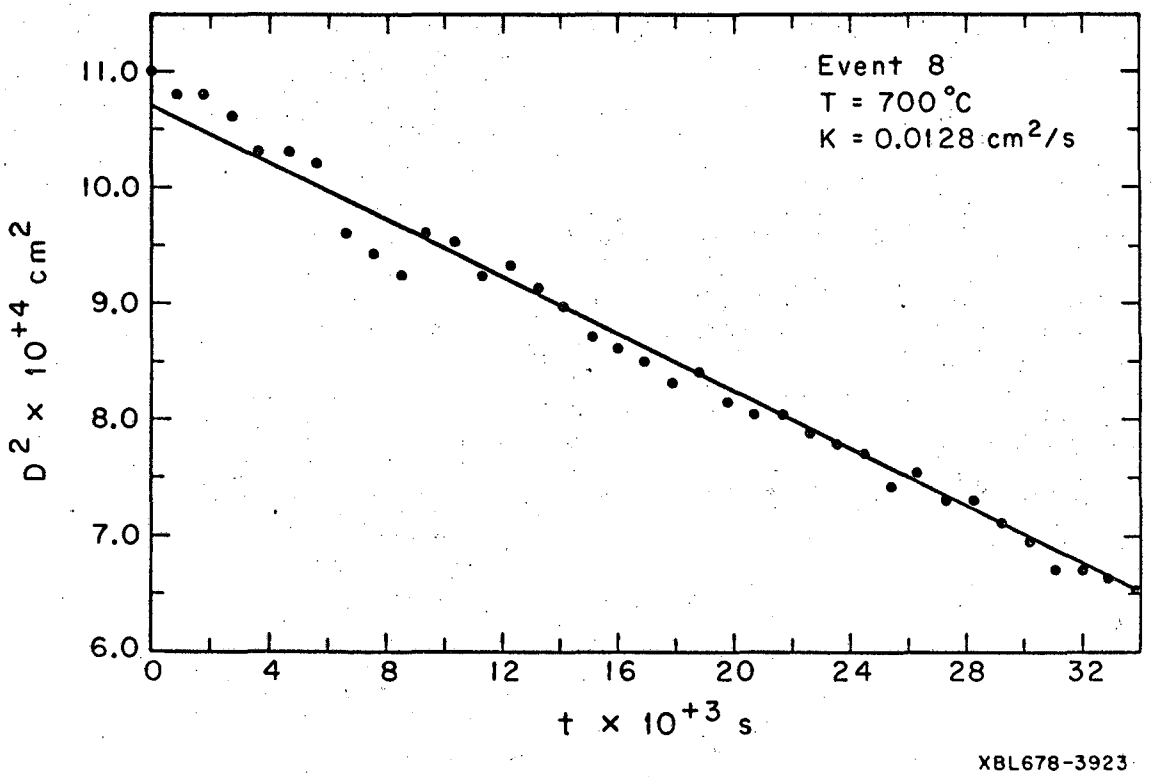

Fig. 14 Diameter squared versus time for a burning droplet of n-heptane (Event 8)

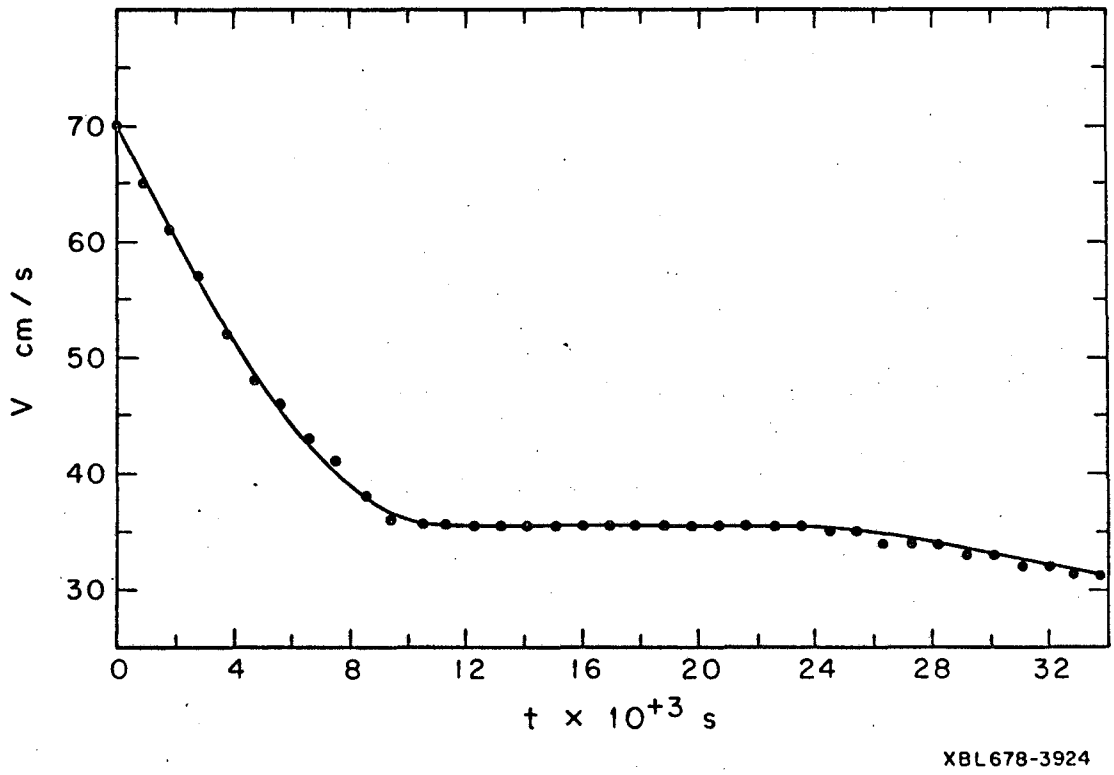

Fig. 15 Velocity versus time for droplet of event 8

XBB 677-4149

Fig. 16 Burning droplet suspended at its terminal velocity

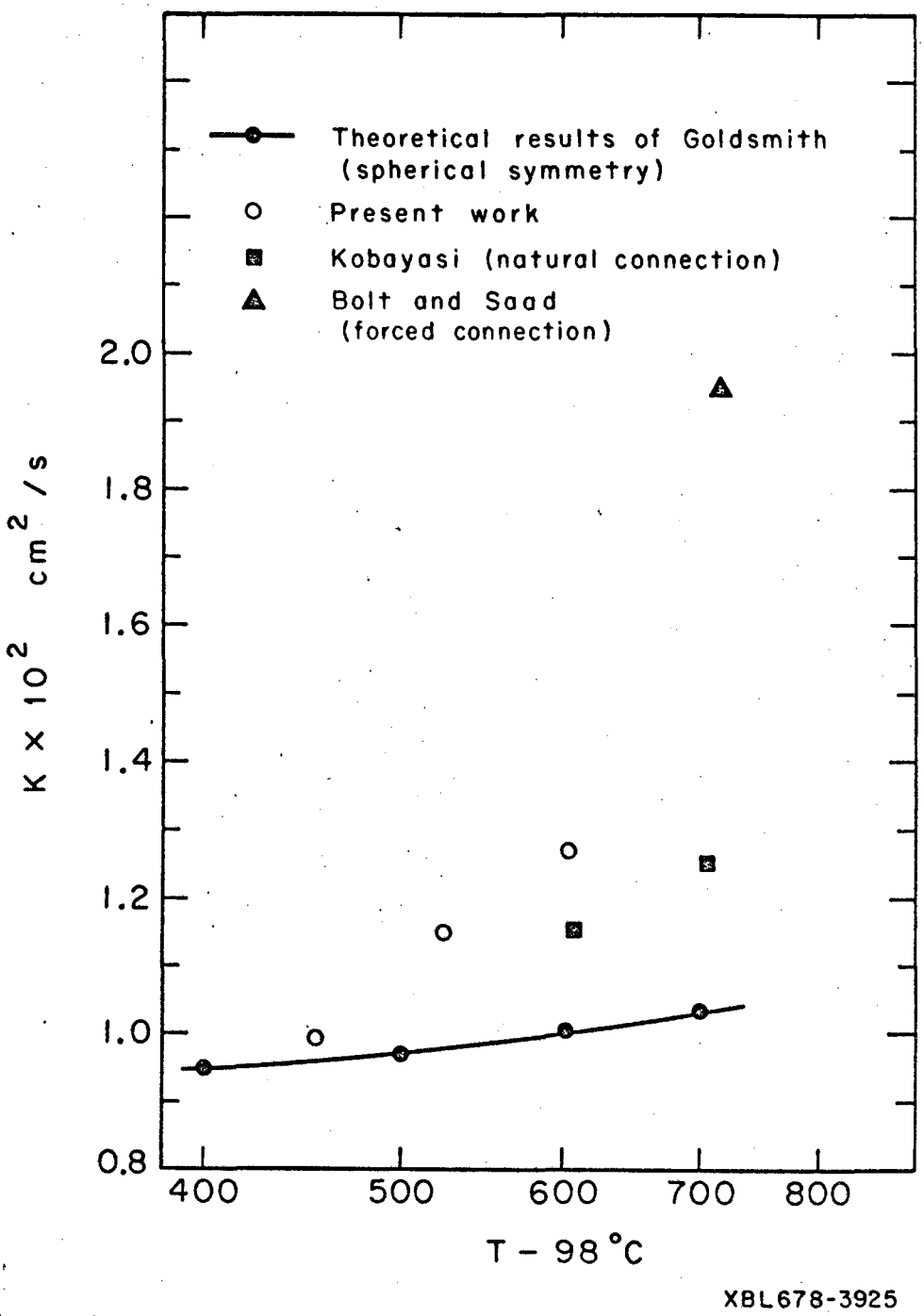

Fig. 17 Burning rate coefficient versus log of environmental temperature minus 98°C.

Table I

Burning rate coefficients as a function of temperature and relative gas velocity.

Event	K cm^2/s	T°C	V_{gas} cm/s	$V_{relative}$ cm/s	$D_{initial}$ μ	D_{final} μ
1	0.0099	550	17	73-60	328 -	276
2	0.0115	620	35.5	35.5	150 -	132
3	0.0112	620	35.5	35.5 - 60	312 -	278
4	0.0125	620	35.5	70 - 50	326 -	279
5	0.0104	620	35.5	65 - 40	229 -	173
6	0.0120	620	35.5	36 - 50	242 -	200
7	0.0125	700	36.1	66	337 -	320
8	0.0128	700	36.1	70 - 30	332 -	256
9	0.0119	700	36.1	88	410 -	380
10	0.0129	700	36.1	66	241 -	221
11	0.0121	700	36.1	56	202 -	167
12	0.0116	700	36.1	70 - 36	269 -	249
13	0.0134	700	36.1	56 - 36	330 -	296
14	0.0140	700	36.1	96	340 -	321
15	0.0122	700	36.1	60	341 -	217

Table II

Burning rate coefficients of various investigators at room temperature.

Investigator	Temperature (°C)	Type	Burning Rate Coefficient
Godsave[1]	20	Experimental	0.0097 cm^2/sec
Kumagai and Isoda[9]	25	Experimental	0.0099 cm^2/sec
Goldsmith[8]	27	Theoretical	0.0086 cm^2/sec
Goldsmith[8]	25	Experimental	0.0084 cm^2/sec
Goldsmith[8†]	25	Experimental	
		Relative Velocity = 11.8 cm/s	0.0102 cm^2/sec
		Relative Velocity = 26.9 cm/s	0.0110
		Relative Velocity = 34.5 cm/s	0.0114
Goldsmith and Penner[3]	27	Experimental	0.0097 cm^2/sec
Agoston, Wood, and Wise[15*]	20	Theoretical	0.0142 cm^2/sec
Agoston, Wood, and Wise[15*]	20	Experimental	0.0280 cm^2/sec

* See Appendix 4.

† Convective cases.

APPENDIX 1

The depth of field of a given lens arrangement is given by Hyzer[22] (p. 147-150) as:

$$D = \frac{2cf^2 \quad (M + 1)}{M^2 f^2 - \Lambda^2 C^2}$$

D = depth of field (mm)

C = circle of confusion of film (mm)

f = focal length of lens (mm)

Λ = f - number or relative aperture opening

M = image magnification

The Fastax WF17 camera as used in the experiments employed the largest aperture openings possible. The film used is DuPont's 931A. From these considerations

C = 10μ or 0.01 mm

f = 101.1 mm

Λ = 22

For M = 1 (1:1 magnification)

D = 0.88 mm

For M = 2-1/2 (2-1/2:1 magnification)

D = 0.25 mm

Depth of field for M = 1 is almost four times as large as for M = 2-1/2.

APPENDIX 2

The plot of diameter squared versus time for 14 of the 15 events from which burning rate coefficients were determined are shown in the following seven pages. A similar plot for the other event, number eight, is shown in Fig. 14. The value of the burning rate coefficient is found as the slope of the straight line relating diameter squared to time.

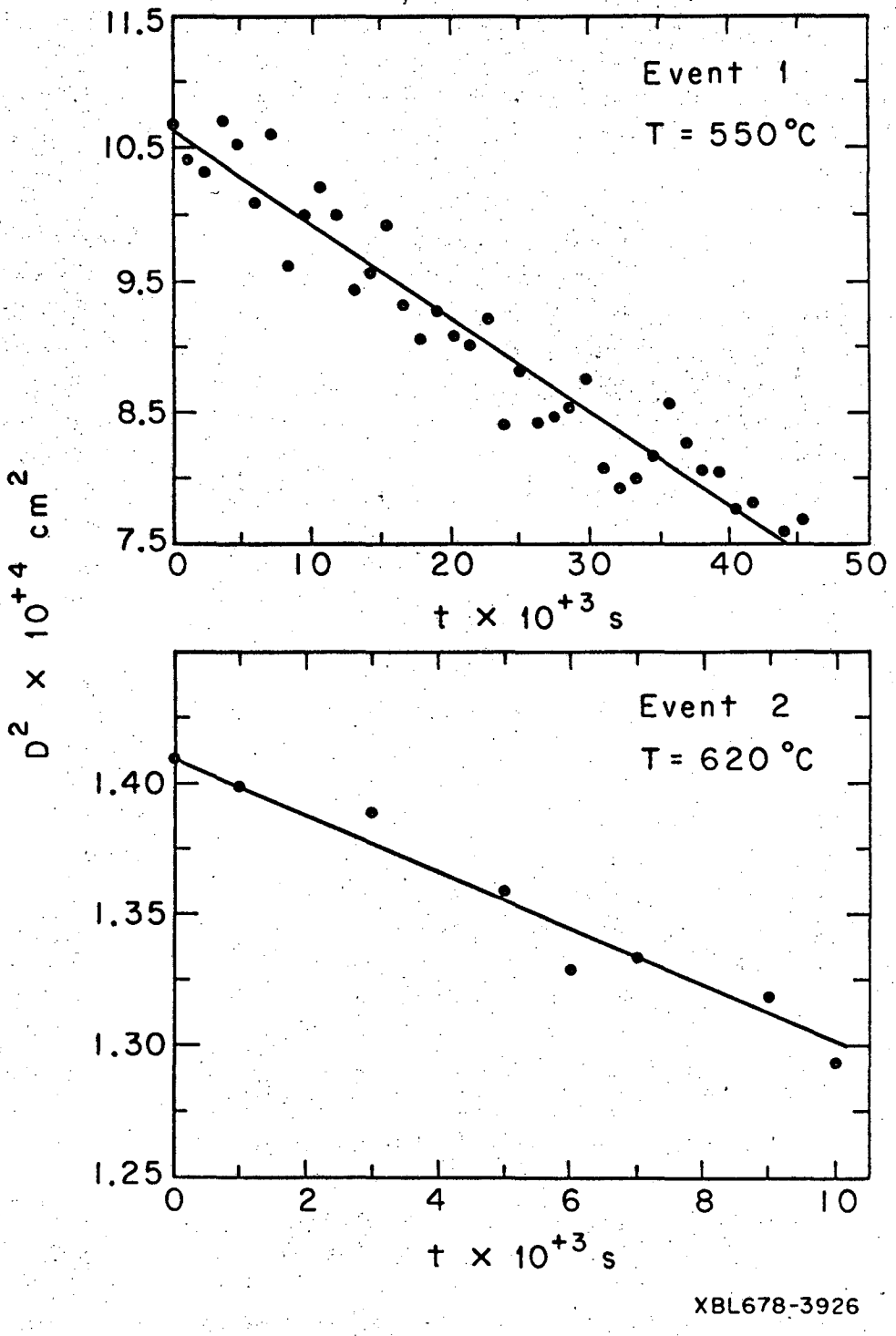
Event 1
T = 550 °C
11.5
10.5
9.5
8.5
7.5
0
10
20
30
40
50
t x 10+3 s
Event 2
T = 620 °C
1.40
1.35
1.30
1.25
0
2
4
6
8
10
t x 10+3 s
D2 x 10+4 cm2
XBL678-3926

Appendix 2-1

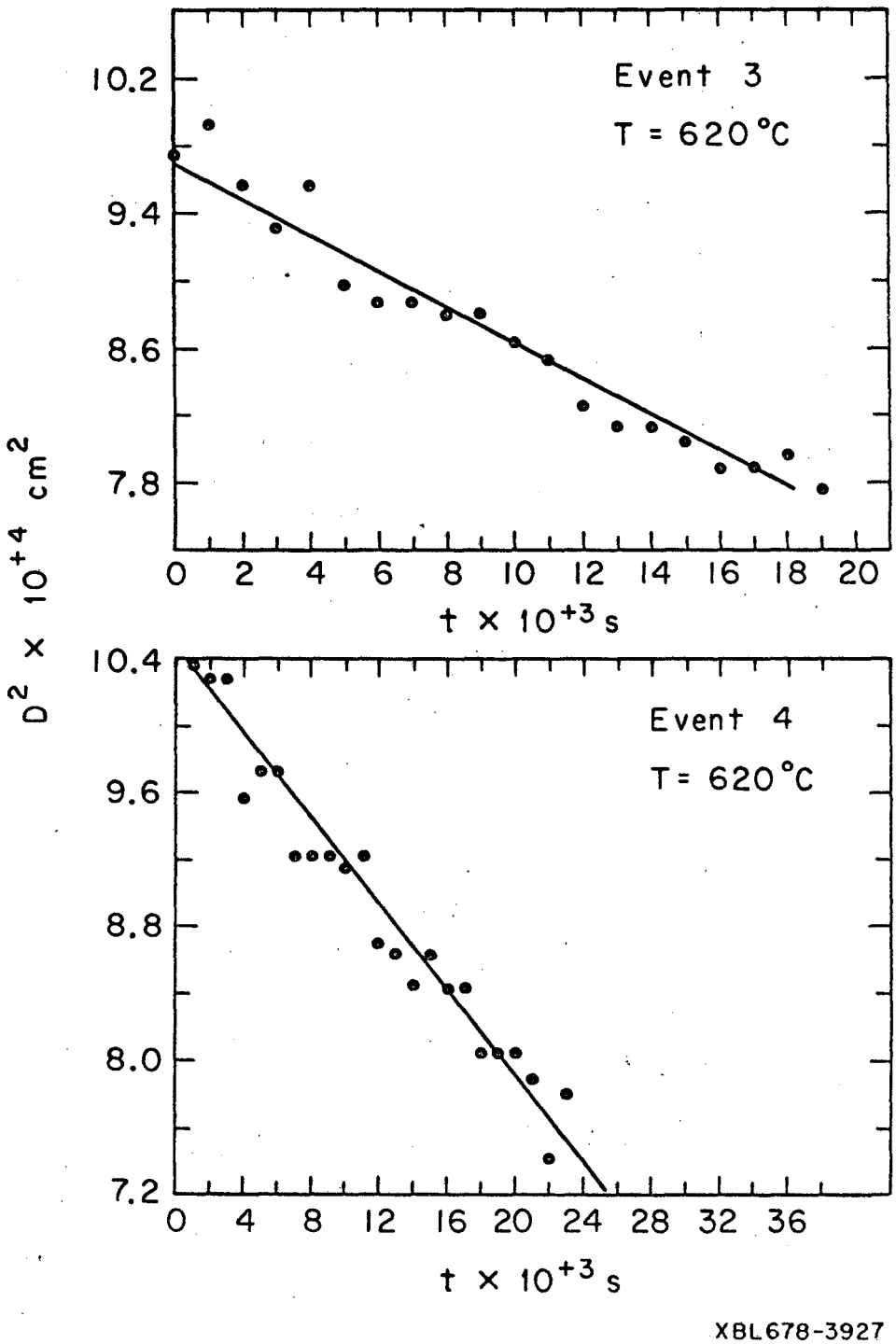
Event 3
T = 620 °C
10.2
9.4
8.6
7.8
0 2 4 6 8 10 12 14 16 18 20
t × 10+3 s
Event 4
T = 620 °C
10.4
9.6
8.8
8.0
7.2
0 4 8 12 16 20 24 28 32 36
t × 10+3 s
D2 × 10+4 cm2
XBL678-3927

Appendix 2-2

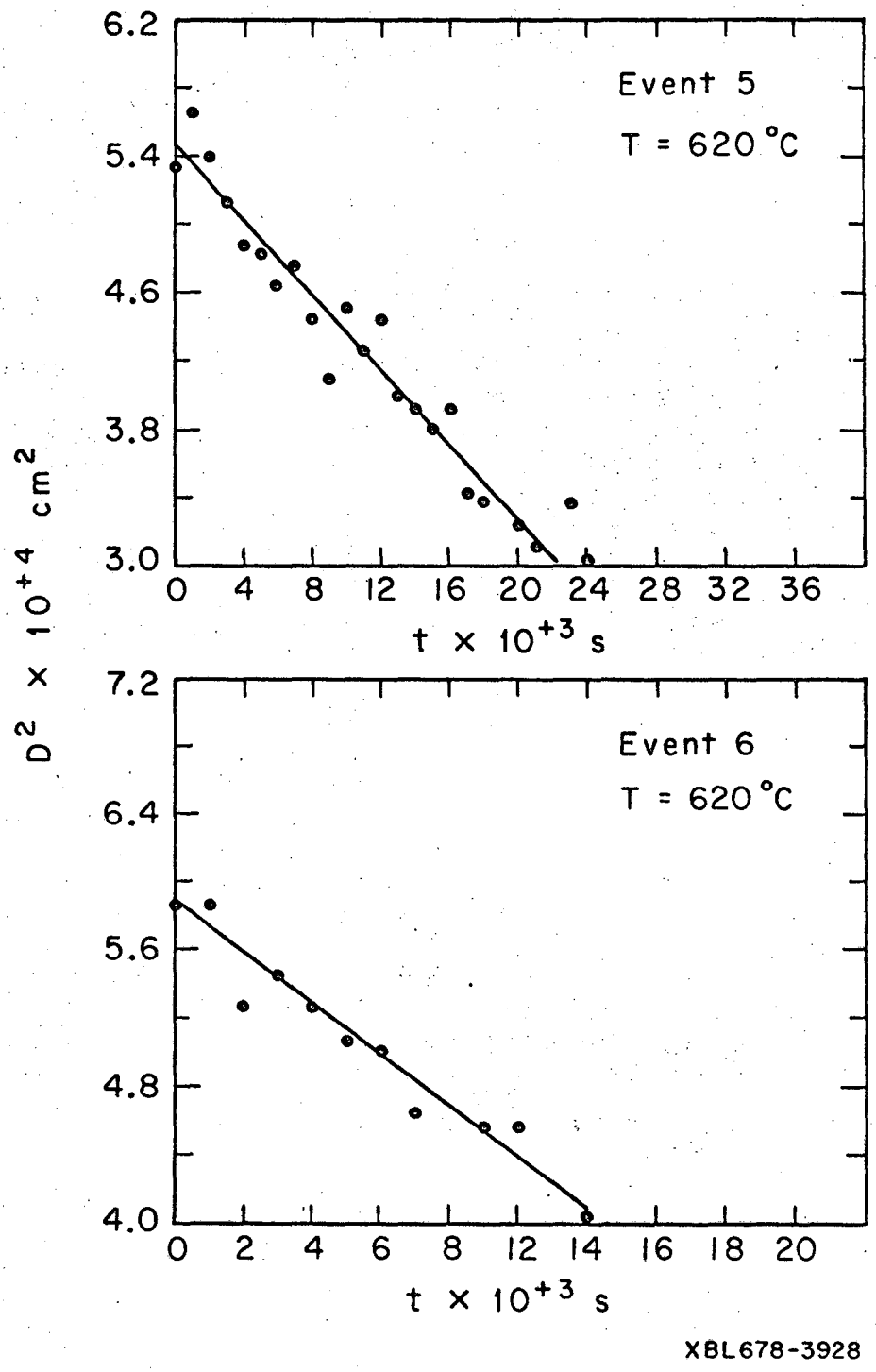
Event 5
T = 620 °C
6.2
5.4
4.6
3.8
3.0
0 4 8 12 16 20 24 28 32 36
t x 10+3 s
Event 6
T = 620 °C
7.2
6.4
5.6
4.8
4.0
0 2 4 6 8 12 14 16 18 20
t x 10+3 s
D2 x 10+4 cm2
XBL678-3928

Appendix 2-3

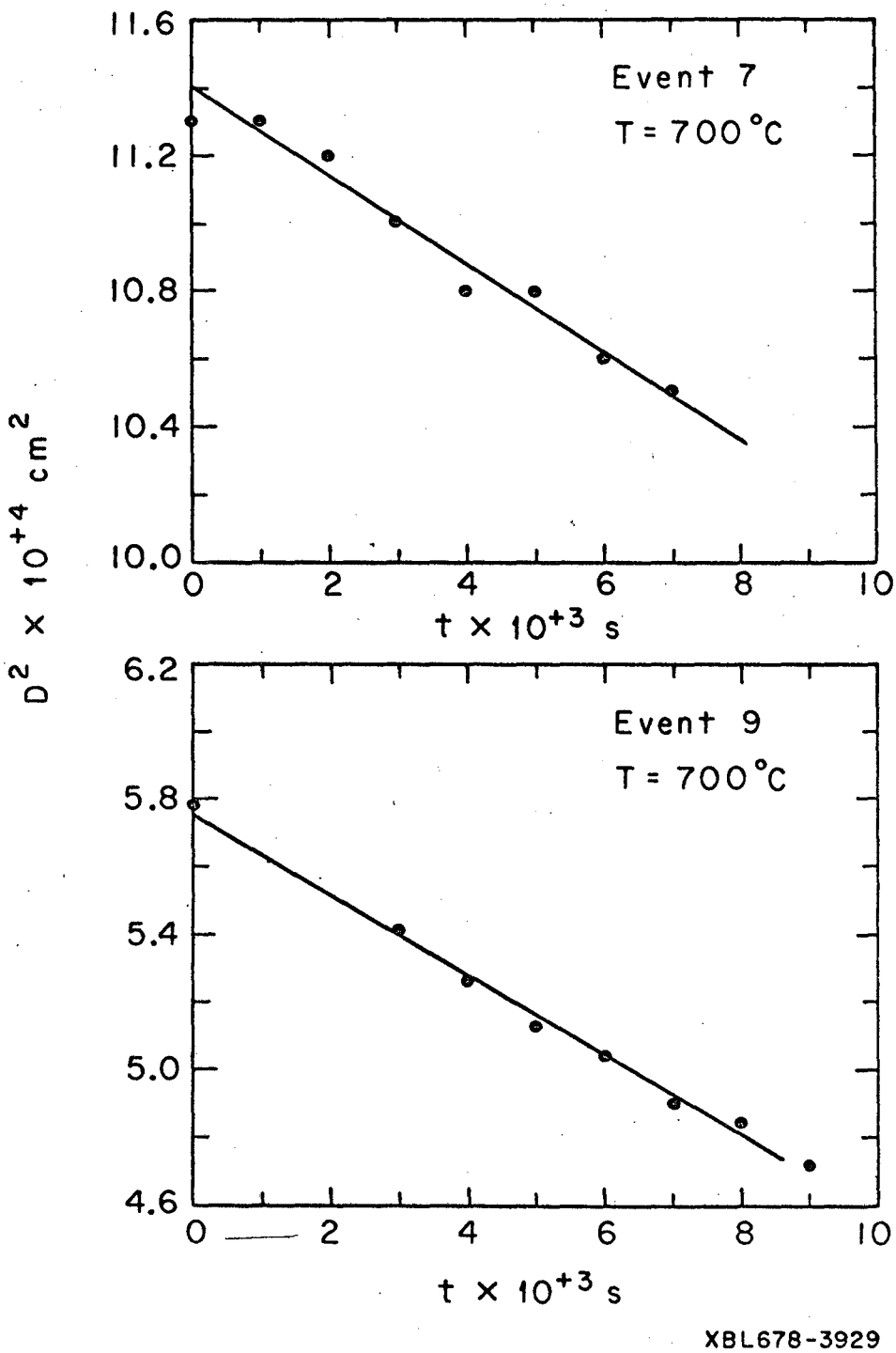
Event 7
T = 700 °C
11.6
11.2
10.8
10.4
10.0
0
2
4
6
8
10
t x 10+3 s
Event 9
T = 700 °C
6.2
5.8
5.4
5.0
4.6
0
2
4
6
8
10
t x 10+3 s
D2 x 10+4 cm2
XBL678-3929

Appendix 2-4

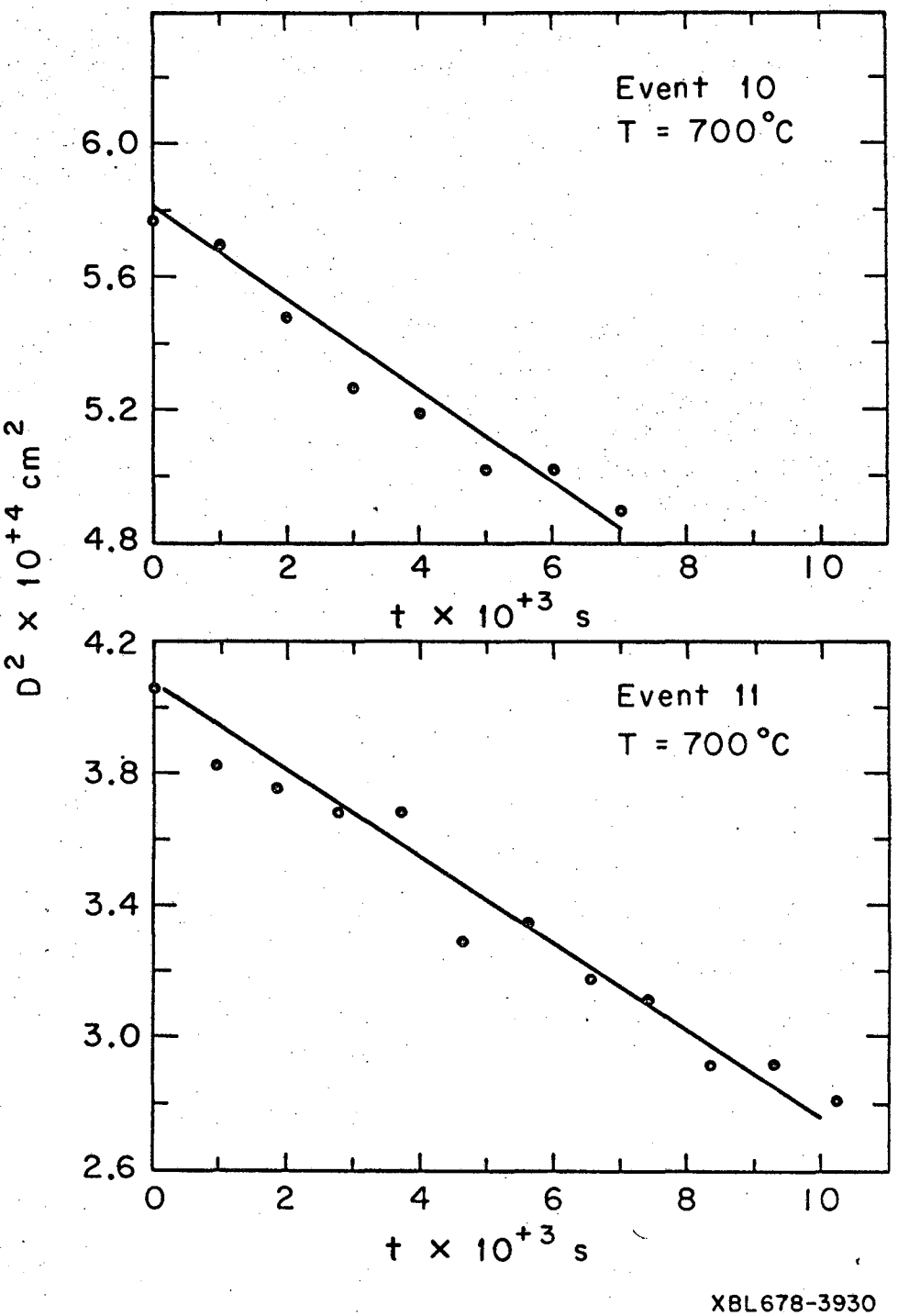
Event 10
T = 700°C
6.0
5.6
5.2
4.8
0
2
4
6
8
10
t × 10+3 s
D2 × 10+4 cm2
Event 11
T = 700°C
4.2
3.8
3.4
3.0
2.6
0
2
4
6
8
10
t × 10+3 s
XBL678-3930

Appendix 2-5

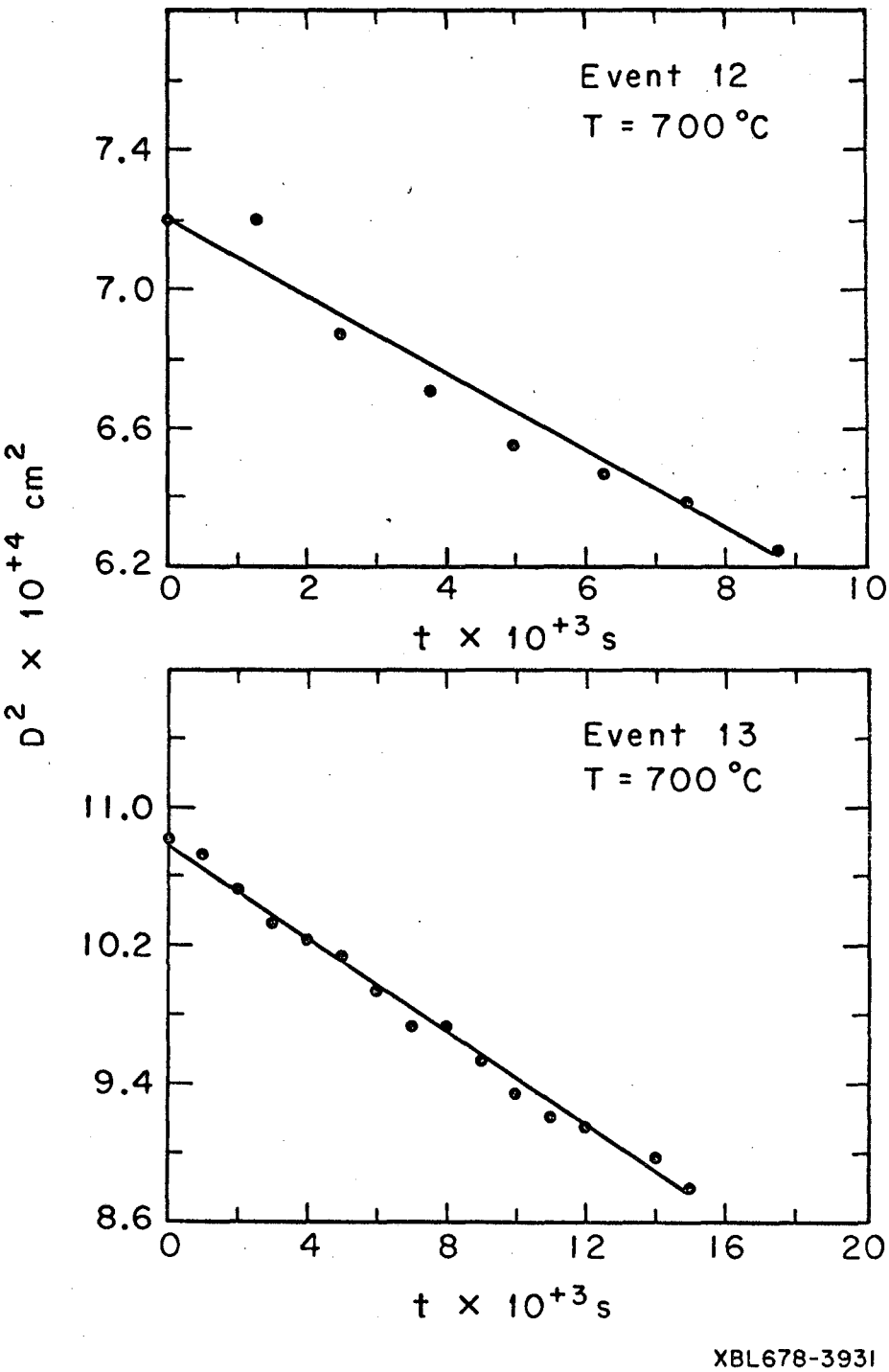
Event 12
T = 700 °C
7.4
7.0
6.6
6.2
0
2
4
6
8
10
t × 10+3 s
D2 × 10+4 cm2
Event 13
T = 700 °C
11.0
10.2
9.4
8.6
0
4
8
12
16
20
t × 10+3 s
XBL678-3931

Appendix 2-6

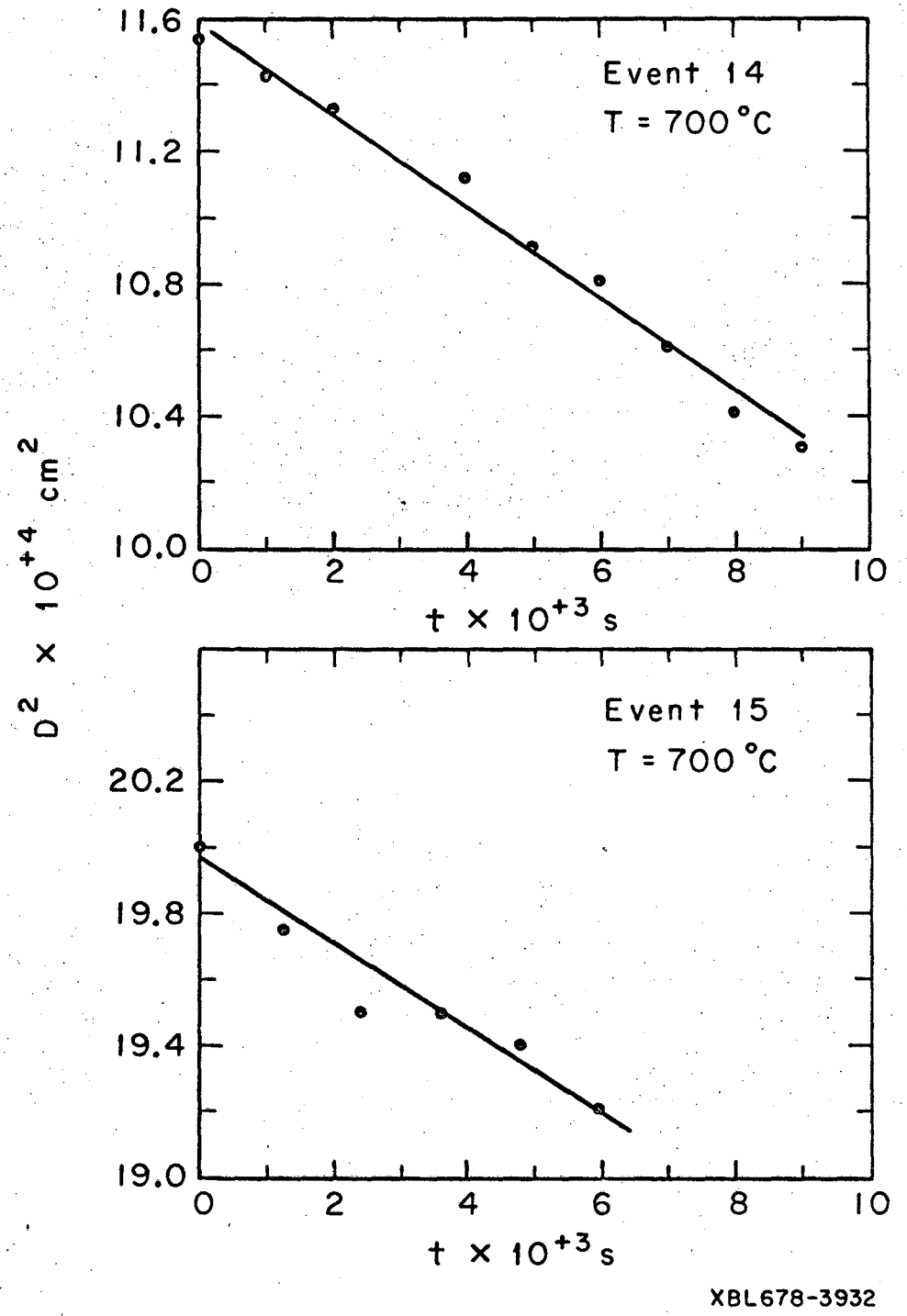
Event 14
T = 700 °C
11.6
11.2
10.8
10.4
10.0
0
2
4
6
8
10
t × 10+3 s
D2 × 10+4 cm2
Event 15
T = 700 °C
20.2
19.8
19.4
19.0
0
2
4
6
8
10
t × 10+3 s
XBL678-3932

Appendix 2-7

APPENDIX 3

Calculation of the Terminal Velocity of a Non-Evaporative Drop

When a drop is falling at its terminal velocity, the force of gravity is balanced by the frictional force: i.e.,

$$F_{friction} = F_{gravity}$$

$$F_{friction} = (\pi r^2)\ (1/2\rho\ V^2)\ (f)$$

where V = terminal velocity (cm/sec)

r = radius of droplet (cm)

ρ = density of gaseous surroundings (g/cm^3)

f = friction factor (dimensionless)

and $F_{gravity} = (4/3)\ \pi r^2 \rho_L g$

where ρ_L = density of liquid droplet (g/cm^3)

g = gravitational constant (cm/s^2)

It is assumed that the velocities necessary to support the drops whose diameter is between 100 and 500μ, shall be in the region classified as Stokes' flow from which $f = 24/Re$ where $Re = 2rV\rho/\mu$, and μ = viscosity of gas (g/cm s). Equating the two forces; substituting f and solving for V one obtains

$$V = (2/9)\rho_L r^2\ g/\mu$$

$\rho_L = 0.617 g/cm^3$ n-heptane at its boiling point under 1 atm pressure.

$r = 70 = 7\times10^{-3}$ cm

$\mu = 3.27\times10^{-4}$ g/cm s evaluated at mean temperature between drop surface (98°C) and free stream at (620°C)

$$g = 980 \text{ cm}^2/\text{s}^2$$

from which $V = 26.3$ cm/s

To check the assumption of Stokes' flow Re is calculated

$$Re = 0.59$$

At Re = 0.59 the Stokes' flow assumption is fair as seen in Bird, Stewart, and Lightfoot,[23] Fig. 6. 3-1 page 192.

APPENDIX 4

Velocity of Evaporating Material at Droplet Surface

The velocity of the evaporating material at the droplet surface can be calculated from the mass rate of change of the drop (dm/dt in g/s), the area of the drop surface (A in cm^2), and the density of the gaseous vapor at the surface of the drop (ρ_V in g/cm^3) according to the formula,

$$dm/dt = -\rho_V AV$$

where $m = (4/3)\pi r^3 \rho_L$ see nomenclature of Appendix 3.

where $A = 4\pi r^2$

so that $\rho_L \, dr/dt = -\rho_V V$ (1)

From the relation for the burning rate coefficient,

$$dD^2/dt = -k \quad \text{or} \quad 4\, dr^2/dt = -k$$

the following can be obtained

$$dr/dt = -k/8r$$

Substituting for dr/dt in Eq. (1):

$$V = 1/8(\rho_L/\rho_V)k/r$$

for $r = 70\mu$

$k = 0.0115 \ cm^2/s$ at $T = 620°C$

$\rho_L = 0.617 \ g/cm^3$

ρ_V is calculated as the density of the gaseous n-heptane at 98.4°C and 1 atm pressure.

From Weber and Meissner[23]

$P = 1$ atm $\qquad T = 98.4°C = 371.7°K$

$P_c = 27$ atm $\qquad T_c = 540.2°K$

$P_r = 0.037 \qquad T_r = 0.69$

$\rho_V = 3.47 \times 10^{-3}$ g.cm^3

so that

$V = 36.5$ cm/sec

APPENDIX 5

Converting Mass Burning Rates into Burning Rate Coefficients

Agoston, Wood, and Wise[15] report their results in the form of mass burning rates. To convert these to burning rate coefficients the following procedure is followed (see Appendix 3 for nomenclature)

$-\dot{m}$ = mass burning rate = dm/dt in g/s

$$-\dot{m} = d/dt(\pi D^3 \rho_L/6) = \pi D \rho_L/4(2D\ dD/dt) \qquad (1)$$

The definition of a burning rate coefficient is:

$$-k = dD^2/dt = 2D\ dD/dt \qquad (2)$$

substituting for 2D dD/dt in Eq. (1)

$$\dot{m} = \pi D \rho_L/4\ k$$

or

$$k = 4\dot{m}/\pi \rho_L D$$

From Agoston, Wood, and Wise[15]

$$\dot{m}/D - 6.88\times10^{-3}\ g/cm\ s \qquad \rho_L = 0.617\ g/cm^3$$

$$k = 1.42\times10^{-2}\ cm^2/s$$

APPENDIX 6

The work of Bolt and Saad is the only other experimental investigation besides the present work under consideration to report burning rate coefficients for free falling droplets travelling at their terminal velocity. They determine burning rate coefficients by obtaining the slope at a particular point of the line representing diameter squared versus time constructed from three pictures each of a number of different size burning droplets falling at their respective terminal velocities. They did not obtain a straight line relationship between diameter squared and time, perhaps because they used different size droplets which were falling at different velocities. The burning rate coefficient that they report for a 300μ n-heptane droplet travelling at a relative velocity of 215 cm/s in air at 815°C is 0.0195 cm^2/s. This burning rate coefficient is much greater than the burning rate coefficients of 0.0124 cm^2/s that Kobayasi determined at 800°C, and 0.0103 cm^2/s that is calculated from the diffusion theory at 815°C. However, if the slope of the line representing the present burning rate coefficients as a function of temperature is extrapolated to include the temperature at which Bolt and Saad report their result, at 815°C, then a burning rate coefficient of 0.0150 cm^2/s would be obtained, a result not too different from Bolt and Saad's result. The convective conditions to which the droplets of Bolt and Saad's experimentation were subjected is characterized by Reynold's numbers greater than one, so that a simplified analysis such as that of Wijffles[17] cannot hold.

REFERENCES

1. G. A. E. Godsave, Fourth Symposium on Combustion, pp.818-829 (1952).
2. D. B. Spalding, Fourth Symposium on Combustion, pp. 847-864 (1953).
3. M. Goldsmith and S. S. Penner, Jet Propulsion 24, 245 (1954).
4. J. Lorell and H. Wise, J. Chem. Phys. 23, 1928 (1955).
5. S. S. Penner, Chemistry Problems in Jet Propulsion (Pergamon Press, New York, 1957), pp. 276-292.
6. F. A. Williams, J. Chem. Phys. 33, 133 (1960).
7. J. Lorell, H. Wise and R. Carr, J. Chem. Phys. 25, 325 (1956).
8. M. Goldsmith, Jet Propulsion 26, 172 (1956).
9. S. Kumagai and H. Isoda, Sixth International Symposium on Combustion. pp. 726-731 (1957).
10. C. Sanchez Tarifa, P. Perez del Notario and F. Garcia Moreno, Eighth International Symposium on Combustion, pp. 1035-1056 (1961).
11. J. A. Bolt and M. A. Saad, Sixth International Symposium on Combustion, pp. 717-725 (1957).
12. R. D. Ingebo, T. N. 3265, 1954.
13. A. G. Agoston, H. Wise, and W. A. Rosser, Sixth International Symposium on Combustion, pp. 708-717 (1957).
14. H. Wise, J. Lorell, and B. J. Wood, Fifth Symposium on Combustion, pp. 132-141 (1954).
15. G. A. Agoston, B. J. Wood, and H. Wise, Jet Propulsion 28, 181 (1958).
16. M. Salabarria, Combustion of Liquid Droplets Entrained in a Hot Gas Stream (M. S. Thesis, University of California, Berkeley, Sept. 1965.
17. J. B. Wijffels, Behavior of Droplets Evaporating in High Temperature Convective Environment (M. S. Thesis), University of California, Berkeley, Sept. 1965.

18. T. C. DuMond, Engineering Materials Manual (Reinhold Pub. Co., New York, 1951).

19. R. Ingebo, Eighth Sympsoium on Combustion, pp. 1104-1113 (1960).

20. K. Kobayasi, Fifth Symposium on Combustion, pp. 141-148 (1954).

21. F. Fendell, M. Sprankle, and D. Dodson, J. Fluid Mech. 26, 267-280 (1966).

22. W. G. Hyzer, Engineering and Scientific High-Speed Photography (Mac-Millan Co., New York, 1962), Chap. 4.

23. R. Bird, W. Stewart, and E. Lightfoot, Transport Phenomena (J. Wiley and Sons, Inc., New York, 1964), Chap. 6.

24. H. Weber and H. Meissner, Thermodynamics for Chemical Engineers (J. Wiley and Sons, Inc., New York, 1959), Chap. 8.